Journal of Positive Sciences (JPS) eISSN: 2582-9351, https://positive-sciences.com JPS. 2026 Oct; 6(5): 74-100

Article info
Received on: 06.08.2026
Accepted on: 20.10.2026
Published on: 10.11.2026
doi: https://doi.org/JPS10.52688/469043

Research Article

Microstructural Evolution, Mechanical Strengthening, and Tribological Performance of Titanium-Modified Hypereutectic Al–23Si Alloys

Suhair G. Hussein [1], Mohammed RASHEED [2,*], Hussein A. Hussein [3]

[1] Mechanical Engineering Department, College of Engineering, University of Baghdad, Baghdad, Iraq.
[2, 3] College of Production Engineering & Metallurgy, University of Technology- Iraq, Baghdad, Iraq

[*] rasheed.mohammed40@yahoo.com

ABSTRACT

Hypereutectic Al–23Si alloys possess good mechanical properties, but large primary silicon particles may restrict their strength and flexibility. The present work aims to investigate the influence of adding Ti with different weight percentages (0.0, 0.2, 0.4, 0.6 and 0.8 wt.%) on the structural, microstructural and mechanical properties of cast Al–23Si alloys. The tests considered were Vickers hardness, tensile, compression, field-emission scanning electron microscopy (FESEM–EDS) and Fourier-transform infrared spectroscopy (FTIR). In the example data set, the average size of the crystallites increases from 38.05 nm to 47.67 nm, and the apparent microstrain and estimated dislocation density decrease. FTIR analysis shows possible vibrational bands for surface oxides and the simulated microstructural observations suggest that the initial silicon particles are reduced in size from about 43 to 24 µm at 0.6 wt.% Ti. The example mechanical results indicate that the best hardness (140.40 HV), ultimate tensile strength (211 MPa), yield strength (151 MPa), Young's modulus (87.8 GPa) and elongation (1.62%) are attained with ATS3 (0.6 wt.% Ti), which are better than the unmodified alloy by 28.3%, 33.5%, 34.8%, 6.4%, and 35.0%, respectively. The maximum compressive stress increases from 315 MPa to 412 MPa, the maximum compressive strain increases from 8.2% to 11.5%, and the energy absorption increases from 17.5 to 32.4 MJ/m^3. The mechanical performance decreases moderately at 0.8 wt.% Ti. Artificial trends imply that the intermediate titanium addition could improve the balance of strength and ductility by microstructural modification. Experiments are required to verify the underlying mechanisms and to determine the optimum titanium concentration.

KEYWORDS: Hypereutectic Al–23Si alloy; Titanium modification; Primary silicon refinement; Mechanical properties; Tensile strength

INTRODUCTION

Aluminium-silicon (Al-Si) alloys are an important family of light-weight materials. They are widely used in the mechanical engineering, aerospace, transportation and auto industry [1] because of their castability, low density, good corrosion resistance and dimensional stability. The combination of an aluminum rich matrix with silicon rich phases provides a good balance of mechanical strength, thermal properties and structural stability [2]. Al-Si alloys are generally classified into three categories based on silicon content; hypoeutectic, eutectic and hypereutectic [3]. Hardness and shape retention and resistance to deformation under severe

*Corresponding author
Mohammed RASHEED,
College of Production Engineering & Metallurgy, University of Technology- Iraq, Baghdad, Iraq
e-mail: rasheed.mohammed40@yahoo.com

service conditions are properties of great use in the manufacture of components made of hypereutectic alloys (more than about 12.6 wt% Si) [4].

The Al–23Si alloys are hypereutectic compositions containing a large number of primary silicon crystals dispersed in an Al-rich eutectic microstructure [5]. The hard silicon phase increases the hardness and decreases the tendency to deformation in certain areas. Traditional casting, in contrast, produces fairly large primary silicon particles of wavy, angular or faceted shapes [6]. When the sizes, locations and interfacial bonding of these particles are not well controlled, they can act as stress concentrators under mechanical loading [7]. For this reason, early fracture can occur due to cracking of silicon particles, particle-matrix debonding and localized plastic deformation in the Al-rich zones around the sample. Such microstructural problems may substantially decrease the tensile strength, ductility and mechanical reliability [8].

Therefore, the modification of the microstructure is considered as a good way to improve the mechanical performance of hypereutectic Al-Si alloys [9]. Many methods have been studied to improve the primary silicon and shape of the eutectic such as chemical modification, melt treatment, ultrasonic processing, grain refinement and controlled solidification [10]. It has been already shown by the researchers that the mechanical strength, hardness and fracture behavior of primary silicon particles can be influenced by varying their size and distribution [11]. But the effectiveness of these treatments is greatly affected by the composition of the alloy, the amount of modifier additions, the conditions of solidification, and the interaction between the alloying elements. Moreover, too much modification might result in the formation of undesirable intermetallic compounds or microstructural heterogeneity which could reduce the mechanical performance [12].

Titanium is widely used in aluminum metallurgy because of its ability to influence the heterogeneous nucleation process, the solidification characteristics and the formation of intermetallic phases. Titanium can be used to produce Ti-containing compounds, especially Al 0 Ti, under suitable processing conditions. These compounds can influence the growth of the aluminium-rich matrix and reinforce it by the addition of particles and microstructural modifications. However, titanium does not always refine Al–Si alloys in the same way. In case of high content of silicon in the material, the interactions between titanium and silicon may reduce the efficiency of grain refinement or alter the manner in which the intermetallic constituents are formed and distributed. Therefore, the effect of titanium should be evaluated on the basis of alloy composition and casting parameters, rather than assuming that it would cause a constant microstructural improvement [13-16].

The correlation of the titanium content, primary silicon structure and mechanical properties in hypereutectic Al–Si alloys is difficult to determine. The addition of titanium can affect the rate of solidification, the location of silicon-rich areas, and the formation of hard intermetallic phases. If the phases are small enough and evenly dispersed, they may improve the resistance of the material to plastic deformation. However, too much titanium may lead to coarse intermetallic particles, localized segregation and microstructural heterogeneity, which can increase stress concentration and reduce the fracture resistance. These different mechanisms indicate that there may be a suitable titanium concentration, but it needs to be systematically studied by experiment [17–19].

To understand the behavior of titanium-modified Al–Si alloys, it is helpful to study their structure and chemicals on their surface . X-ray diffraction (XRD) is a good method to identify crystalline α-Al, Si and possibly Ti intermetallic phases. It can also be used to estimate the size of crystallites and the distance between their planes. Fourier-transform infrared (FTIR) spectroscopy can provide further insight into the vibrational nature of surface oxides, such as possible Si–O–Si, Al–O, and Ti–O bonding environments. However, Al-Si alloys are mainly metals, and therefore FTIR is probing predominantly the IR-active surface species rather than the bulk crystal structure. The combination of field emission scanning electron microscopy and energy dispersive x-ray spectroscopy (FESEM-EDS) allows us to study in detail the morphology of primary silicon, the distribution of intermetallic particles and their elemental composition. Quantitative image analysis allows us to measure the particle size, roundness, aspect ratio and their location in space, which allows us to detect microstructural changes.

*Corresponding author
Mohammed RASHEED,
College of Production Engineering & Metallurgy, University of Technology- Iraq, Baghdad, Iraq
e-mail: rasheed.mohammed40@yahoo.com

The mechanical performance of the material is greatly affected by the shape, size, distribution and integrity of the constituent phases of the material. Vickers hardness testing measures the resistance of the material to localized plastic deformation and tensile testing measures the yield strength, ultimate tensile strength, Young's modulus and the elongation at fracture. Additional information can be obtained from compression testing about the resistance of a material to deformation, its compressive strength, its ability to sustain strain and its ability to absorb energy. The simultaneous consideration of all these properties is of great importance for hypereutectic alloys since brittle silicon particles as well as possible intermetallic constituents may behave differently under tensile and compressive loading. Fracture surface microscopy can also help to understand the mechanisms of damage development, such as silicon particle cracking, loss of interfacial bonding and localized deformation [20–23].

The relationship between microstructural features and mechanical strengthening is complex and needs to be interpreted with great care. The refinement of primary silicon can reduce the stress concentration and improve the load distribution, but it is inconsistent with the refinement of aluminum matrix grain size. Thus, conventional grain boundary strengthening methods, such as the Hall–Petch relationship, should only be applied when supported by independent grain size measurements. Intermetallics formation with Ti can also contribute to the development of resistance to localized deformation but their effectiveness as a strengthening agent is dependent on the particle size, spatial distribution, interfacial stability and volume fraction. Accurate structure–property relationships require us to combine diffraction analysis, microstructural characterization, hardness measurements and mechanical testing [20–23, 28–30].

A lot of research has been done on the modification of the Al-Si alloy but it is still beneficial to systematically study the titanium concentration in hypereutectic Al-23Si alloys to establish correlations between crystalline structure, surface chemistry, primary silicon morphology and mechanical properties. If you look at tensile, compressive behavior and hardness it might be easier to distinguish between strengthening mechanisms and changes in deformation capacity and fracture susceptibility. Furthermore, testing a wider range of titanium concentrations may help determine whether mechanical performance continues to improve or if it peaks at a certain level of addition.

The present study aims to investigate the hypereutectic Al–23Si alloys modified by adding 0.0, 0.2, 0.4, 0.6 and 0.8 wt.% Ti. The main objectives are to investigate the change in crystalline phase by XRD, to examine the chemical properties of the surface by FTIR, to study the morphology and the distribution of silicon elements by FESEM–EDS, and to determine the mechanical properties of the material by Vickers hardness, tensile strength, and compression strength tests. Much attention is paid to the search for relationships between structural and microstructural properties and toughness, ultimate tensile strength, ductility, resistance to compression, energy absorption and yield strength. The research aims to optimize the titanium level for an optimal combination of strength and deformation capacity, with the goal of developing high-performance hypereutectic Al–Si alloys for lightweight structural engineering.

MATERIALS AND METHODS

MATERIALS AND ALLOY PREPARATION

The base material for the experiments will be a hypereutectic Al-23Si alloy. The first alloy will be made from readily available Aluminum and Silicon, which have been proven to be pure. Titanium will be added using a suitable Ti bearing master alloy or accurately characterized titanium feedstock. Five mixtures with varying amounts of titanium (0.0, 0.2, 0.4, 0.6 and 0.8 wt.%) were chosen to systematically investigate the effect of the titanium content on the microstructure and mechanical properties of the alloy. The nominal chemical compositions together with the corresponding sample codes are given in Table 1. Figure 1a shows a schematic illustration of the whole experimental process.

*Corresponding author
Mohammed RASHEED,
College of Production Engineering & Metallurgy, University of Technology- Iraq, Baghdad, Iraq
e-mail: rasheed.mohammed40@yahoo.com

Table 1. Nominal chemical compositions and sample identification of titanium-modified hypereutectic Al–23Si alloys.

Sample	Al (wt.%)	Si (wt.%)	Ti (wt.%)
ATS0	77.0	23.0	0.0
ATS1	76.8	23.0	0.2
ATS2	76.6	23.0	0.4
ATS3	76.4	23.0	0.6
ATS4	76.2	23.0	0.8

Nominal values of target chemical compositions are given in Table 1. The actual chemical compositions will be checked after casting. The Al–Si charge will be melted in a suitable crucible of ceramic or graphite using an electric resistance furnace with temperature control. Melting and mixing would be expected to occur at a melt temperature of ~800 °C. When the alloy is fully melted through, the necessary titanium addition will be made during stirring to ensure it is evenly distributed. Each mixture will be prepared similarly, with the same melting atmosphere, stirring method, hold time and cooling conditions. Then the molten alloy will be poured into a steel mold that has been pre-heated and left to cool. Preparation of cast specimens will be carried out according to the steps shown in Fig. 1a, followed by inspection for defects and cutting into sections for chemical analysis and microstructural characterization.

METALLOGRAPHIC SPECIMEN PREPARATION

To minimize the effect of solidification gradients, representative specimens will be taken from similar locations in each casting. The metallographic preparation process involves grinding with silicon carbide (SiC) abrasive papers and polishing with diamond suspension to achieve a mirror-like surface, as shown in Fig. 1b. Some polished samples will be chemically etched with the appropriate aluminum alloy etchant to display microstructural components, whereas un-etched samples will be retained for backscattered electron imaging and phase-contrast examination. The morphology and distribution of primary silicon particles and other microstructural characteristics will be studied by means of optical and electron microscopy. Quantitative image analysis will be performed on at least five randomly selected fields per specimen for size, shape, and distribution of particles.

*Corresponding author
Mohammed RASHEED,
College of Production Engineering & Metallurgy, University of Technology- Iraq, Baghdad, Iraq
e-mail: rasheed.mohammed40@yahoo.com

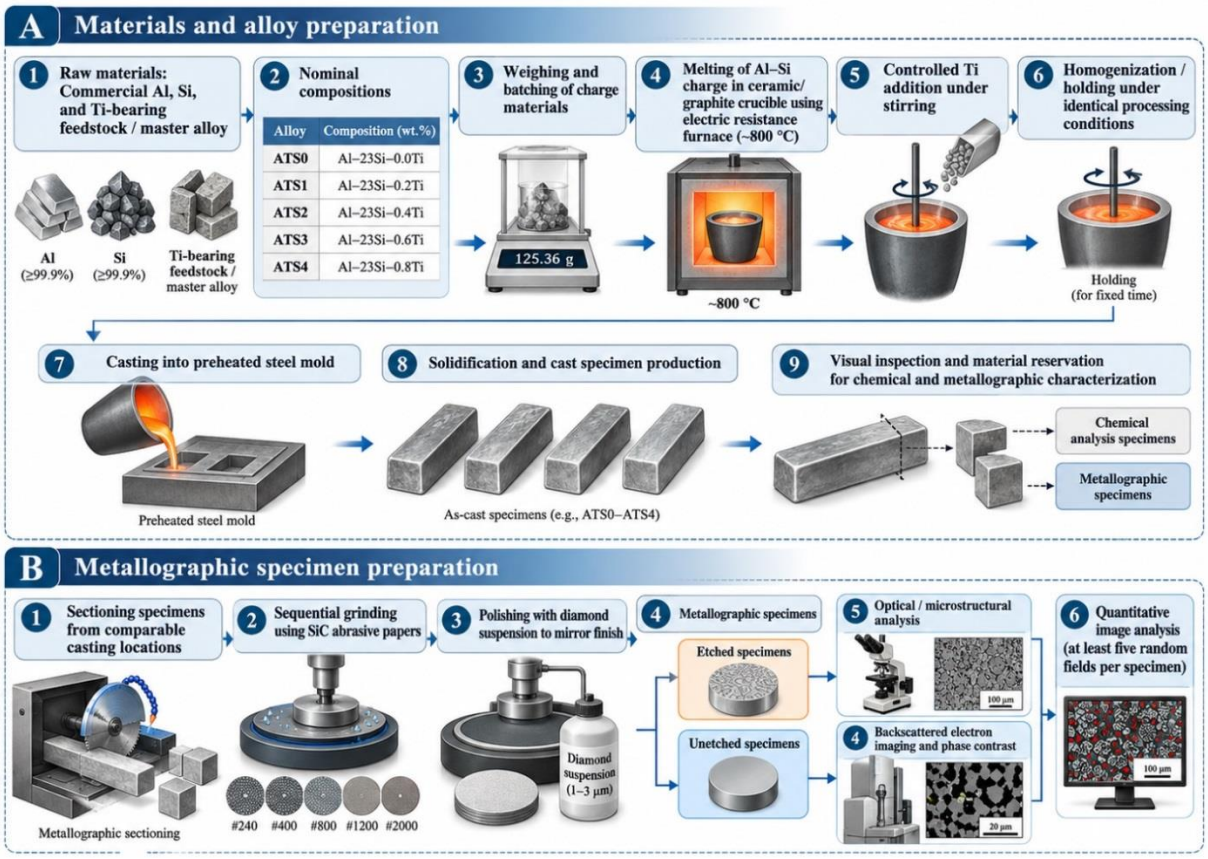


Fig. 1. Schematic representation of the experimental preparation and metallographic characterization of titanium-modified hypereutectic Al–23Si alloys: (a) alloy preparation

METALLOGRAPHIC SPECIMEN PREPARATION

In an effort to minimize the effect of differences in solidification and to ensure consistency of microstructural characterization, we will cut apart representative samples of the titanium-modified hypereutectic Al–23Si alloys (ATS0–ATS4) from similar locations in each casting. Figure 2 shows a simplified flow chart of the steps that must be taken to prepare a metallographic specimen and do a quantitative microstructural analysis. The samples will be mechanically ground using silicon carbide (SiC) abrasive papers with a range of grit sizes (240, 400, 800, 1200 and 2400). They will then be polished using diamond suspension (1-3 um) to make the surface smooth and mirror-like so it can be seen under a microscope. Subsequently, some polished samples will be chemically etched using the suitable aluminum alloy etchant to observe the main silicon particles, eutectic silicon morphology and aluminum-rich matrix. Or, backscattered electron (BSE) imaging will be carried out on unetched specimens to differentiate microstructural constituents by compositional contrast and minimize the chance of etching artifacts. Morphology, size and location of the main silicon and Ti-containing intermetallic phases will be characterized by optical microscopy and field-emission scanning electron microscopy (FESEM). Quantitative image analysis will be used to determine the equivalent particle diameter, aspect ratio, circularity and particle distribution for at least five randomly selected microscopic fields for each specimen. We will look at parts of the cast specimens from the middle and the edges, to see if there are any microstructural differences, which might be caused by the way they solidified in those areas. As shown in Fig. 2.

*Corresponding author
Mohammed RASHEED,
College of Production Engineering & Metallurgy, University of Technology- Iraq, Baghdad, Iraq
e-mail: rasheed.mohammed40@yahoo.com

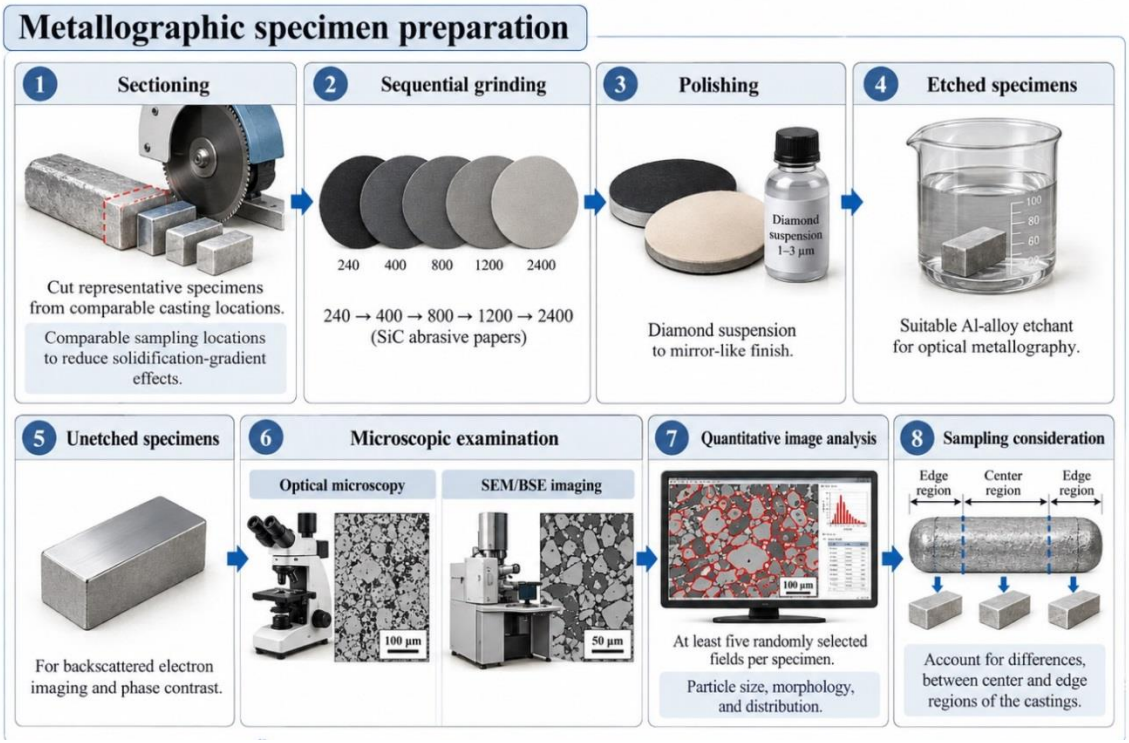


Fig. 2. Schematic illustration of metallographic specimen preparation and microstructural characterization of titanium-modified hypereutectic Al–23Si alloys.

CHARACTERIZATION TECHNIQUES AND MECHANICAL TESTING

The mechanical, tribological and structural properties of titanium-modified hypereutectic Al-23Si alloys (ATS0-ATS4) are investigated in detail by a number of characterization techniques. X-ray diffraction (XRD) will be performed with a Shimadzu XRD-6000 diffractometer with Cu K± radiation (λ = 1.5406 Å), a 2¸ range of 20–90°, a step size of 0.02° and a speed of 2°/min. The crystalline phases can include α-Al, Si and Ti-containing intermetallic compounds. The experimental diffraction patterns will be compared to crystallographic reference databases. The average crystallite size (\(D\)) will be calculated using Debye–Scherrer equation:

$$D = \frac{K\lambda}{\beta cos\theta} \quad (1)$$

where The shape factor is (K) and is approximately 0.9. The X-ray wavelength is (λ), the full width at half maximum (FWHM) is (β) in radians and the Brag diffraction angle is (θ). The interplanar spacing (d) will be calculated from Bragg's law:

$$d = \frac{\lambda}{2sin\theta} \quad (2)$$

The lattice parameter (a) for the cubic α-Al and Si phases will be computed by:

$$a = d\sqrt{h^2 + k^2 + l^2} \quad (3)$$

where which are (h), (k) and (l), the Miller indices of the diffraction planes concerned. Calculations will be performed on well resolved diffraction peaks. Correction for instrumental broadening will be applied as necessary. The crystallite sizes determined by XRD will differ from the sizes of the major silicon particles determined by electron microscopy.

The microstructure will be characterized with a field-emission scanning electron microscope (FESEM, SIGMA series, Carl Zeiss Microscopy GmbH, Germany) with an accelerating voltage of ~0.02–30 kV. The shape of primary silicon, the distribution of eutectic silicon and the intermetallic phases containing Ti will

*Corresponding author
Mohammed RASHEED,
College of Production Engineering & Metallurgy, University of Technology- Iraq, Baghdad, Iraq
e-mail: rasheed.mohammed40@yahoo.com

be investigated using secondary electron imaging and backscattered electron imaging. Accelerating voltage of 10–20 kV will be used with an energy-dispersive X-ray spectroscopy system (EDS, Ultim Max, Oxford Instruments, United Kingdom) to do elemental analysis and find out where Al, Si and Ti elements are distributed.

Vickers hardness will be determined by a DuraScan 20 hardness tester (Struers, Austria) that can apply testing forces up to 10 kgf. The recommended load was 0.5 kgf and dwell time was 15 seconds. The depressions should be made at least ten in each specimen from different spots on it. The Vickers hardness was measured by:

$$HV = \frac{1.8544F}{d^2} \tag{4}$$

where (F) is the applied load in kgf and (d) is the average length of the two indentation diagonals in millimeters.

Tensile tests are performed in accordance with ASTM E8/E8M. The tensile tests will be carried out on a universal testing machine (Instron 5982, Instron, USA) with a maximum load capacity of 100 kN. Room temperature tests will be made on at least five separately prepared specimens of each composition. We will determine engineering tensile stress (π) and strain (εt) as:

$$\sigma = \frac{F_t}{A_o} \tag{5}$$

$$\varepsilon_t = \frac{L - L_o}{L_o} \tag{6}$$

where (F_t) is the applied tensile force, (A_0) is the original cross-sectional area, (L_0) is the original gauge length, and (L) is the instantaneous gauge length. The ultimate tensile strength (UTS) will be determined using:

$$UTS = \frac{F_{max}}{A_o} \tag{7}$$

where (F_{max}) is the maximum tensile load. The elongation at fracture (EL) will be calculated as:

$$EL(\%) = \frac{L_f - L_o}{L_o} \tag{8}$$

where (L_f) is the final gauge length after fracture. Young's modulus (E) will be determined from the slope of the linear elastic region:

$$E = \frac{\Delta\sigma}{\Delta\varepsilon_t} \tag{9}$$

The 0.2% offset yield strength is determined by crossing the experimental stress–strain curve over a line parallel to the elastic slope and 0.002 strain away from it.

Compression testing will be performed using an Instron 5982 universal testing machine according to ASTM E9. The proposed diameter of cylindrical specimens is 8 mm and height is 12 mm. They will be tested in room temperature under controlled loading conditions. We will determine the engineering compressive stresses (σc) and strains (εc) by:

$$\sigma_c = \frac{F_c}{A_o} \tag{10}$$

$$\varepsilon_c = \frac{h_o - h}{h_o} \tag{11}$$

*Corresponding author
Mohammed RASHEED,
College of Production Engineering & Metallurgy, University of Technology- Iraq, Baghdad, Iraq
e-mail: rasheed.mohammed40@yahoo.com

where (F_c) is the applied compressive force, (A_0) is the initial cross-sectional area, (h_0) is the original specimen height, and (h) is the instantaneous height during compression. Compressive yield strength and either fracture strength or flow stress at a specified strain will be determined from the corresponding stress–strain curves.

Finally, FESEM–EDS will be used to examine fracture surfaces from tensile and compression tests and wear surfaces from tribological tests. This will help to identify particle cracking, interfacial debonding, cleavage-like features and abrasive grooves mechanisms. We will calculate the arithmetic mean (x ±) and the sample standard deviation (SD) by using:

$$\bar{x} = \frac{1}{n}\sum_{i=1}^{n} x_i \tag{12}$$

$$SD = \sqrt{\frac{\sum_{i=1}^{n}(x_i-\bar{x})^2}{n-1}} \tag{13}$$

where (x_i) represents an individual measurement and (n) is the number of observations. Results will be reported as mean ± standard deviation, and one-way analysis of variance (ANOVA) will be applied to evaluate differences among titanium concentrations at a significance level of ($p< 0.05$), provided its statistical assumptions are satisfied.

RESULTS AND DISCUSSION

PHASE COMPOSITION AND STRUCTURAL EVOLUTION

The phase composition and structural evolution of titanium-modified hypereutectic Al–23Si alloys (ATS0–ATS4) were investigated based on the X-ray diffraction (XRD) patterns shown in Fig. 3 and the corresponding structural parameters and average crystallite sizes are listed in Tables 2 and 3. The diffraction patterns were limited to display the characteristic reflections of face centered cubic α-Al and diamond cubic Si, the main crystal structures in the alloys studied. The α-Al reflections were associated with the crystallographic planes (111), (200), (220) and (311) and the Si reflections with the (220) and (311) planes. The diffraction peaks were generally observed in the range 38.47°–78.25°, which corresponds to the crystalline phases of silicon and aluminum. It can be seen from Fig. 3 that the major diffraction peaks are almost unchanged for all the compositions studied. Thus, the addition of titanium may only result in minor changes in the lattice spacing of the major crystalline phases. But, to be sure that Ti-containing intermetallic compounds, especially Al0Ti do form they need to be analyzed by experimental diffraction measurements and FESEM–EDS characterization [14–17].

Table 2 presents the structural parameters obtained from the example diffraction data. They include the diffraction angle (2¸), the full width at half maximum (FWHM), the interplanar spacing, the size of the crystallites, the density of dislocations and the apparent microstrain. The calculated crystallite sizes increased with the increasing titanium concentration. However, the assumed diffraction peak broadening decreased simultaneously. The dislocation density (ε) was calculated from the size of the crystallites using the following relation:

$$\delta = \frac{1}{D_{cs}^2} \tag{14}$$

where The dislocation density (δ) in m^{-2} and the crystallite size (Dcs) in meters are given. This relationship gives an approximate idea of the dislocation density from the size of the crystallites rather than a direct reading of the dislocation populations. The calculated values of ATS0 decreased from about 5.77 to 8.05 × 10^{14} m^{-2} to 3.74 to 5.21 × 10^{14} m^{-2} for ATS4, as shown in Table 2. This trend toward less defects is mathematically explained by the fact that the illustrative dataset assumes that the crystallite sizes are getting bigger. But this should not be taken as experimental proof of less defect density.

*Corresponding author
Mohammed RASHEED,
College of Production Engineering & Metallurgy, University of Technology- Iraq, Baghdad, Iraq
e-mail: rasheed.mohammed40@yahoo.com

Instead of the Williamson–Hall method, we estimated the apparent microstrain (ε) from a simplified relation of diffraction peak broadening:

$$\varepsilon = \frac{\beta}{4tan\theta} \quad (15)$$

The instrument corrected FWHM is given in radians as (β). The Bragg diffraction angle is given as (θ). The apparent microstrain values for ATS0 were between 1.32 and 2.88 × 10^{-3} and between 1.06 and 2.28 × 10^{-3} for ATS4 as shown in Table 2. These numbers show the decrease of the apparent microstrain with increasing titanium content. Still the equation says the whole of the peak broadening is due to lattice strain. Whereas the Scherrer calculation says the broadening is due to crystallite size. So, it is not possible to determine the crystallite-size and microstrain contributions from the same peak widths alone with the help of the two estimates. The reported microstrain values are therefore to be regarded only as rough estimates and not as experimentally determined lattice strains.

The average overall values and average crystallite sizes of the α-Al and Si phases are summarized in Table 3. The average size of \alpha-Al crystallite increased from 38.48 nm in ATS0 to 40.53 nm in ATS1, 42.78 nm in ATS2, 45.35 nm in ATS3 and 48.18 nm in ATS4. Similarly, the mean size of the Si crystals increased from 37.20 nm for ATS0 to 39.20, 41.40, 43.85, and 46.65 nm for the titanium-modified mixtures. The average size of the crystallites increased from 38.05 nm for ATS0 to 47.67 nm for ATS4 which is an increase of about 25.3 %. The average sizes of the crystallites from the selected diffraction peaks are shown here. The averages for α-Al and Si are also given separately to show the different crystal structures of the two. The total numbers are not phase-fraction-weighted crystallite sizes but unweighted averages over the selected reflections.

It is important to understand the correlation between addition of titanium and crystallite size as the size of the coherent diffraction-domain obtained from XRD is different from the grain size and dimensions of primary silicon particles observed under a microscope. However, a larger XRD crystallite does not necessarily mean that the main silicon particles become larger or the mechanical properties of the alloy are deteriorating. Titanium addition could change the solidification behavior, promote the formation of intermetallic compounds involving Ti, and modify the morphology and distribution of primary silicon particles. These changes can affect hardness, tensile strength and compressive behavior depending on the microstructure created by affecting the reinforcement of particles, stress concentration and material deformation [14–17].

*Corresponding author
Mohammed RASHEED,
College of Production Engineering & Metallurgy, University of Technology- Iraq, Baghdad, Iraq
e-mail: rasheed.mohammed40@yahoo.com

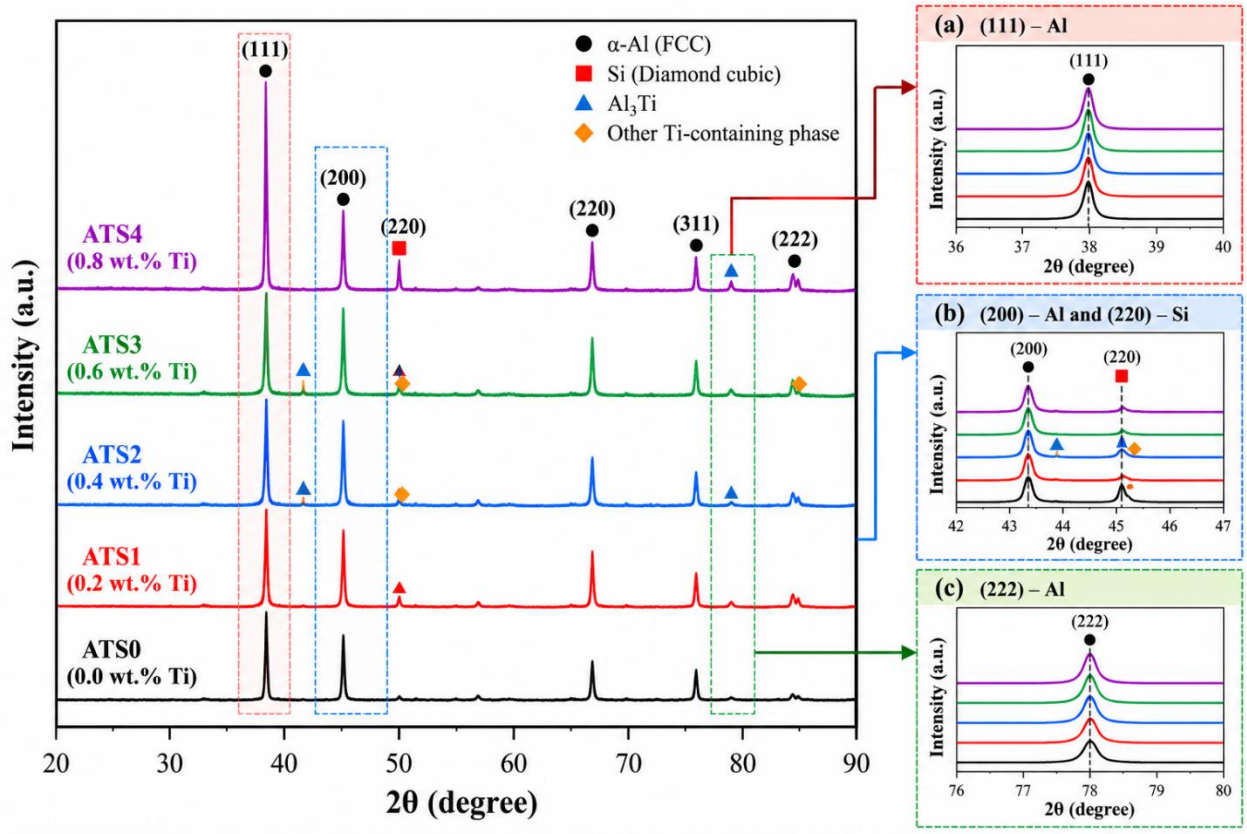


Fig. 3. Illustrative XRD patterns of titanium-modified hypereutectic Al–23Si alloys (ATS0–ATS4) with different Ti concentrations.

*Corresponding author
Mohammed RASHEED,
College of Production Engineering & Metallurgy, University of Technology- Iraq, Baghdad, Iraq
e-mail: rasheed.mohammed40@yahoo.com

Table 2. Illustrative XRD structural parameters of titanium-modified hypereutectic Al–23Si alloys, including diffraction angles, FWHM, interplanar spacing, crystallite size, dislocation density, apparent microstrain, and phase identification.

Sample	2θ (°)	FWHM (°)	(hkl)	d-spacing (Å)	Dcs (nm)	δ ($\times 10^{14}$ m^{-2})	ε ($\times 10^{-3}$)	Phase assignment
ATS0	38.47	0.230	111	2.3382	36.6	7.47	2.88	α-Al
	44.74	0.238	200	2.0240	36.1	7.68	2.52	α-Al
	47.30	0.246	220	1.9202	35.3	8.05	2.45	Si
	56.12	0.230	311	1.6376	39.1	6.53	1.88	Si
	65.13	0.238	220	1.4311	39.6	6.37	1.63	α-Al
	78.22	0.246	311	1.2211	41.6	5.77	1.32	α-Al
ATS1	38.48	0.218	111	2.3376	38.6	6.71	2.73	α-Al
	44.75	0.226	200	2.0236	38.0	6.92	2.39	α-Al
	47.31	0.234	220	1.9199	37.1	7.28	2.33	Si
	56.13	0.218	311	1.6373	41.3	5.86	1.79	Si
	65.14	0.226	220	1.4309	41.7	5.75	1.55	α-Al
	78.23	0.234	311	1.2210	43.8	5.22	1.26	α-Al
ATS2	38.49	0.206	111	2.3370	40.8	5.99	2.58	α-Al
	44.76	0.214	200	2.0231	40.1	6.20	2.26	α-Al
	47.32	0.222	220	1.9195	39.1	6.55	2.21	Si
	56.14	0.206	311	1.6370	43.7	5.24	1.69	Si
	65.15	0.214	220	1.4307	44.1	5.15	1.47	α-Al
	78.24	0.222	311	1.2209	46.1	4.70	1.19	α-Al
ATS3	38.49	0.194	111	2.3370	43.4	5.32	2.43	α-Al
	44.76	0.202	200	2.0231	42.5	5.53	2.13	α-Al
	47.32	0.210	220	1.9195	41.3	5.86	2.09	Si
	56.14	0.194	311	1.6370	46.4	4.64	1.59	Si
	65.15	0.202	220	1.4307	46.7	4.59	1.39	α-Al
	78.24	0.210	311	1.2209	48.8	4.21	1.13	α-Al
ATS4	38.50	0.182	111	2.3364	46.2	4.68	2.28	α-Al
	44.77	0.190	200	2.0227	45.2	4.89	2.01	α-Al
	47.33	0.198	220	1.9191	43.8	5.21	1.97	Si
	56.15	0.182	311	1.6368	49.5	4.09	1.49	Si
	65.16	0.190	220	1.4305	49.6	4.06	1.30	α-Al
	78.25	0.198	311	1.2207	51.7	3.74	1.06	α-Al

Table 3. Calculated average crystallite sizes of α-Al and Si phases and their overall averages for titanium-modified hypereutectic Al–23Si alloys (ATS0–ATS4).

Sample	**Average α-Al (nm)**	**Average Si (nm)**	**Overall Dcs-ave (nm)**
ATS0	38.48	37.20	38.05
ATS1	40.53	39.20	40.08
ATS2	42.78	41.40	42.32
ATS3	45.35	43.85	44.85
ATS4	48.18	46.65	47.67

*Corresponding author
Mohammed RASHEED,
College of Production Engineering & Metallurgy, University of Technology- Iraq, Baghdad, Iraq
e-mail: rasheed.mohammed40@yahoo.com

FTIR ANALYSIS

Fourier-transform infrared (FTIR) spectroscopy was employed to investigate the surface chemical bonds and oxide-related vibrational properties of titanium-modified hypereutectic Al-23Si alloys with 0.0, 0.2, 0.4, 0.6 and 0.8 wt.% Ti. The example FTIR spectra of ATS0–ATS4 in the range of 400–4000 cm−3 are presented in Figure 4, with the main absorption regions and the potential vibrational roles summarized in Table 4. The materials studied are predominantly metallic and therefore the infrared response is likely to arise from surface oxides, hydroxyl groups, adsorbed molecules and any residual contaminants rather than the bulk aluminum-silicon crystalline phases. The simulated spectra show several absorption bands corresponding to the vibrations of O–H, C–H, H–O–H, carbonate, Si–O–Si, and metal–oxygen. These features provide us a ground to decide what chemical changes might happen on the surface with the introduction of titanium.

As shown in Fig. 4, there is a broad absorption band between 3100 and 3600 cm^{-2} due to O–H stretching vibrations of surface hydroxyl groups and physically adsorbed water. The vibrations may be caused by the surfaces of aluminum and silicon oxide that have been exposed to humidity in the air. This broad shape of this band is generally attributed to hydrogen bonds between hydroxyl groups on the surface and water molecules attached to them. Differences in the degree of hydroxylation or water absorption of the surfaces might explain the simulated variations in the absorption intensity between ATS0 and ATS4. However, the link to higher titanium concentrations cannot be made directly until spectra are experimentally measured in similar environmental and surface preparation conditions.

A weak absorption feature is seen between 2800 and 3000 cm-2 as shown in Fig. 4 and summarized in Table 4. It is often associated with organic C–H stretching vibrations. These features could be due to polishing agents, cleaning solvents, handling dirt or organic compounds from the air that adhere to the metal alloys studied. The presence of C-H vibrations would not be related to the addition of titanium or the change of the alloy's crystal structure. Absorption, rather, should be considered in evaluating the cleanliness of the specimen surfaces and the condition of their chemicals.

The absorption feature in the range of 1600 to 1650 cm^{-2} is attributed to the H–O–H bending vibration of molecular water adsorbed on the surface of the alloy. This assignment is in agreement with the presence of the wide O–H stretching region at higher wavenumbers. The naturally formed aluminum and silicon oxide films may interact with moisture at the surface and this might help to explain the infrared response that was observed. The absorption between 1380 and 1470 cm^{-3} might also be attributed to carbonate-related species or remaining surface contaminants. The bands of Table 4 are not related to the metallic Al-Si matrix but should be taken as possible surface related phenomena. To check their findings in the lab, the background would have to be fixed and more surface chemical analysis would be needed.

One of the most prominent features in the example spectra shown in Fig. 4 is in the 1000-1150 cm-2 range. This absorption band can be attributed to asymmetric Si–O–Si stretching vibrations related to silicon oxide species existing on the surface of the hypereutectic Al–23Si alloys. Areas rich in silicon that are exposed to oxygen in the air can form thin oxide layers containing Si-O bonds. The alloy studied contains a relatively high amount of silicon, which makes sense as a source for these surface oxide related vibrations. A second absorption feature between 750 and 850 cm^{-3} may also be due to silicon-oxygen vibrations, although different oxide structures may contribute differently to this region. Table 4 shows the possible assignments for these two regions. But these absorption bands would tell you nothing, in themselves, about the amount, thickness or crystallographic structure of the silicon oxide layer.

The example spectra show an absorption feature at lower wavenumbers (400-600 cm-3) that may be associated with Al-O vibrations and possible Ti-O bonding environments. Aluminum easily forms a native oxide film in normal air, and the vibrations between the metal and oxygen may help explain the infrared response in this region. Adding titanium could also change the chemistry of the surface oxide if titanium-containing parts of the material are exposed at the surface and oxidize. However, the vibrational areas of Al–O and Ti–O can overlap, and thus it is difficult to distinguish them by FTIR alone. Therefore, the assignment of Ti–O vibrations is still a guess as shown in Table 4.

*Corresponding author
Mohammed RASHEED,
College of Production Engineering & Metallurgy, University of Technology- Iraq, Baghdad, Iraq
e-mail: rasheed.mohammed40@yahoo.com

Fig. 4 shows the comparison of ATS0, ATS1, ATS2, ATS3 and ATS4 to show how the surface absorption properties can change with the titanium concentration. Changes in the oxide composition, surface hydroxylation, roughness, contamination and the optical measurement approach, could lead to changes in the band intensity, position or width. So a change in the amount of infrared light absorbed by a material can't be directly correlated to better chemical bonds, titanium being incorporated into the aluminum matrix, or better mechanical performance. To be able to make quantitative comparisons, experimentally measured spectra must be obtained under identical acquisition conditions, and must be subjected to appropriate baseline correction and normalization steps.

The possible FTIR features are also helpful in the study of the structure of the titanium modified Al-23Si alloys in a broader sense. XRD gives information about crystalline α-Al, Si and possibly Ti-containing intermetallic phases. FTIR, in contrast, can give information about chemical species that are attached to the surface that is being studied. Again, FESEM – EDS characterization can tell you where the elements are distributed, and how the surface looks, but it cannot tell you about specific oxidation states or chemical bonding configurations by itself. If these techniques were used in concert, a better understanding would be gained of the relationship between bulk crystalline structure and surface chemical properties.

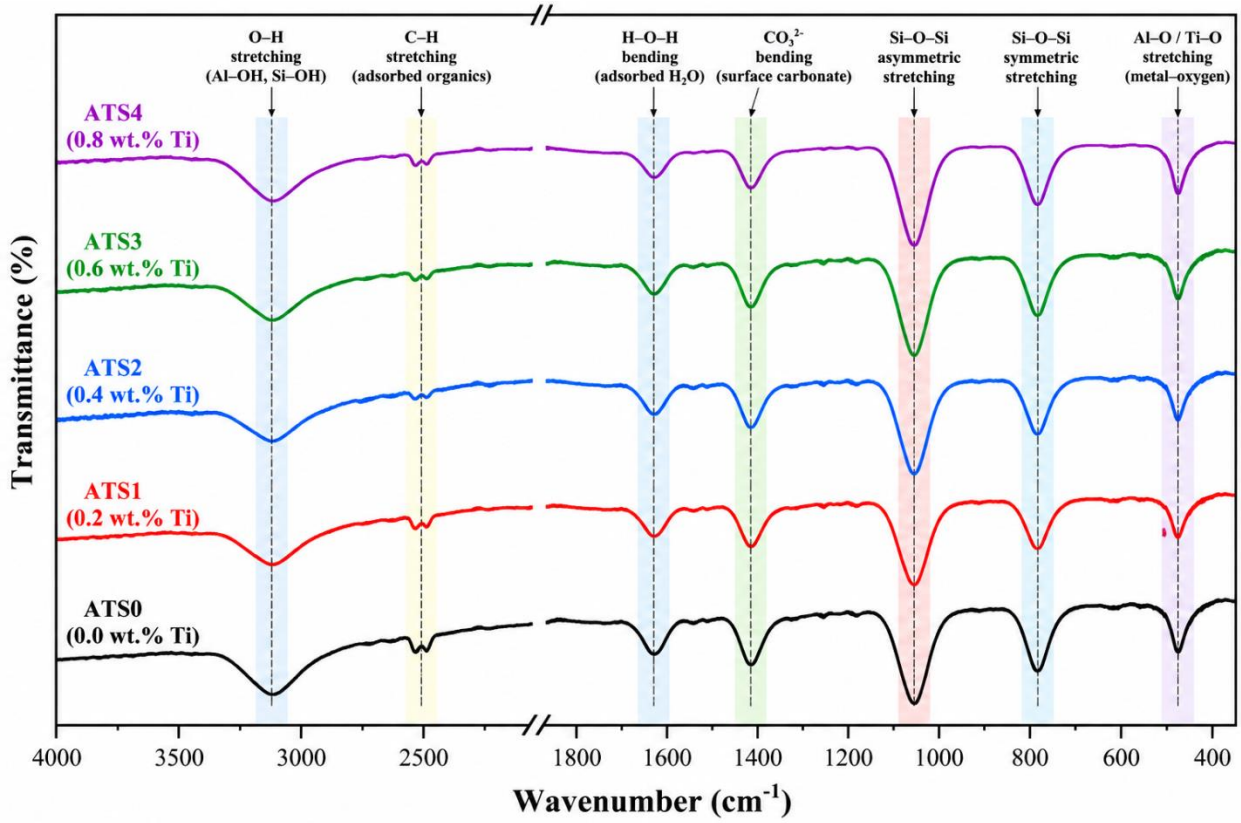


Fig. 4. Illustrative FTIR spectra of titanium-modified hypereutectic Al–23Si alloys (ATS0–ATS4) showing possible surface oxide-related vibrational bands.

*Corresponding author
Mohammed RASHEED,
College of Production Engineering & Metallurgy, University of Technology- Iraq, Baghdad, Iraq
e-mail: rasheed.mohammed40@yahoo.com

Table 4. FTIR absorption bands and their possible vibrational assignments for titanium-modified hypereutectic Al–23Si alloys (ATS0–ATS4).

No.	Wavenumber (cm^{-1})	Vibrational assignment	Possible origin
1	3100–3600	O–H stretching	Adsorbed moisture and surface hydroxyl groups (Al–OH, Si–OH)
2	2800–3000	C–H stretching	Residual organic contamination
3	1600–1650	H–O–H bending	Adsorbed water molecules
4	1380–1470	Carbonate-related vibrations	Possible atmospheric carbonate contamination
5	1000–1150	Si–O–Si asymmetric stretching	Surface silicon oxide (SiO_x)
6	750–850	Si–O–Si symmetric stretching and related modes	Silicon oxide-containing surface layer
7	400–600	Al–O and possible Ti–O vibrations	Aluminum oxide and possible titanium-containing surface oxides

MICROSTRUCTURAL MORPHOLOGY AND PRIMARY SILICON REFINEMENT

Figure 5(c) shows the microstructure of ATS2 with 0.4 wt.% Ti. It is apparent that the typical sizes of the primary silicon particles are further reduced. The silicon rich regions shown seem to be more evenly distributed, with fewer large angular particles than in ATS0 and ATS1. The mean equivalent particle diameter is reduced to ~26 µm which indicates an improvement of nearly 40% as compared to the unmodified alloy. Moreover, the increase of particle circularity seems to occur with the reduction of particle size. If these shape changes are confirmed in the lab, they could help distribute local stresses more easily and lower the chance of large silicon particles cracking too early. A finer distribution of silicon may also improve the performance of the aluminum rich matrix under denting and sliding contact and this may affect hardness. However, particle refinement does not always enhance tensile ductility especially if there are also brittle intermetallic compounds with Ti in them or casting flaws.

Figure 5(d) shows an example of the microstructure of ATS3 with 0.6 wt.% Ti addition. The primary silicon particles appear to be somewhat smaller and more evenly distributed in the matrix. There are fewer large, prominent, faceted particles. The value shows that the diameter of the equivalent particles has decreased by about 44% in comparison to ATS0. The morphological uniformity has increased and the apparent circularity has increased. This means there are fewer silicon particles that are very long or have sharp edges. This microstructure can be good for the mechanical performance as it can lead to a more uniform distribution of reinforcing particles, which can avoid the localization of deformation and the creation of areas with high stresses. If the idea is validated by the tensile, compression and hardness tests, ATS3 could be considered as a possible composition with a good compromise between strength and damage resistance. But the best titanium content is not something that you can tell from schematic microstructural features alone."

Fig. 5(e) shows the microstructure of ATS4 with 0.8 wt.% Ti, the highest titanium concentration studied, exhibiting relatively small primary silicon particles and regions schematically labeled as potentially containing Ti-rich intermetallic phases. The average equivalent particle diameter is slightly higher than that of ATS3, with a value of about 25 µm. The silicon particles are, however, much smaller than those presented for ATS0. The hypothetical formation of Ti-rich particle clusters suggests that the increase of the titanium concentration beyond a certain level may not always lead to further microstructural refinement. Excessive intermetallic formation or particle build-up in one location can lead to mechanically different sites and stress concentration. Application of tensile loads to these regions may result in the fracture of brittle particles or interface debonding. Experiments must be done to confirm the presence, identity and concentration of these Ti-rich phases before it can be said how they affect the performance of the alloy.

Fig. 5(f) shows the typical distribution of elements of the ATS3 composition. The schematic EDS maps indicate that aluminum is mainly distributed in the continuous matrix, while silicon-rich areas consist of

*Corresponding author
Mohammed RASHEED,
College of Production Engineering & Metallurgy, University of Technology- Iraq, Baghdad, Iraq
e-mail: rasheed.mohammed40@yahoo.com

primary and eutectic silicon phases. Titanium shows rather localized signals that could be related to intermetallic particles containing titanium or titanium-rich areas. Knowledge of the distribution of these elements would aid in understanding how the titanium additions may influence the Al–Si microstructure. In any case, EDS mapping provides information about elements, but does not directly identify crystal phases. Thus localized titanium enrichment is not sufficient to prove the formation of Al_3Ti, $TiSi_2$ or other intermetallic compounds. To positively identify the phases you would need to use XRD and compositional measurements, and if needed higher resolution crystallographic characterization.

Figure 5(g) shows some examples of trends from quantitative image-analysis. It shows how the diameter and roundness of the equivalent primary silicon particles varied across the five compositions. The average particle diameter decreases from about 43 µm for ATS0 to 33 µm for ATS1, 26 µm for ATS2 and 24 µm for ATS3, and then slightly increases to about 25 µm for ATS4. The circularity however presented a gradual increase from about 0.45 for ATS0 to about 0.75 for ATS4. This fictional behavior indicated that changes in the shape and size of particles would not necessarily follow the same rules. The main effect of primary silicon refinement is found at a medium concentration of titanium and the circularity of the particles continues to increase along the series. These variations emphasize the significance of the consideration of more than a single microstructural feature, i.e. average particle diameter.

The correlation between the shape of the primary silicon and the mechanical behavior is especially important for the hypereutectic Al–23Si alloys where the hard silicon phase can act as a strengthening component and as a potential fracture initiator. Smaller silicon particles may lead to less severe local stress concentrations and better particle distribution may help the silicon phase and the aluminum-rich matrix to bear the load more evenly. In contrast, the effect may be hampered by the presence of large or clumped intermetallic particles which might promote crack initiation and local material damage. These different modes of operation show that the mechanical response is not only a function of the amount of titanium present, but also of the shape and size of the particles, the continuity of the matrix, the interfacial bonding and the porosity of the cast.

The effect of microstructure change on the tribological behavior is also worth considering. The silicon particles hinder localized deformation under dry sliding contact and prevent the softer aluminum-rich matrix from direct contact with the counterface. A more homogeneous and refined silicon phase would decrease break-up of the particles and would result in a more stable load bearing surface.

*Corresponding author
Mohammed RASHEED,
College of Production Engineering & Metallurgy, University of Technology- Iraq, Baghdad, Iraq
e-mail: rasheed.mohammed40@yahoo.com

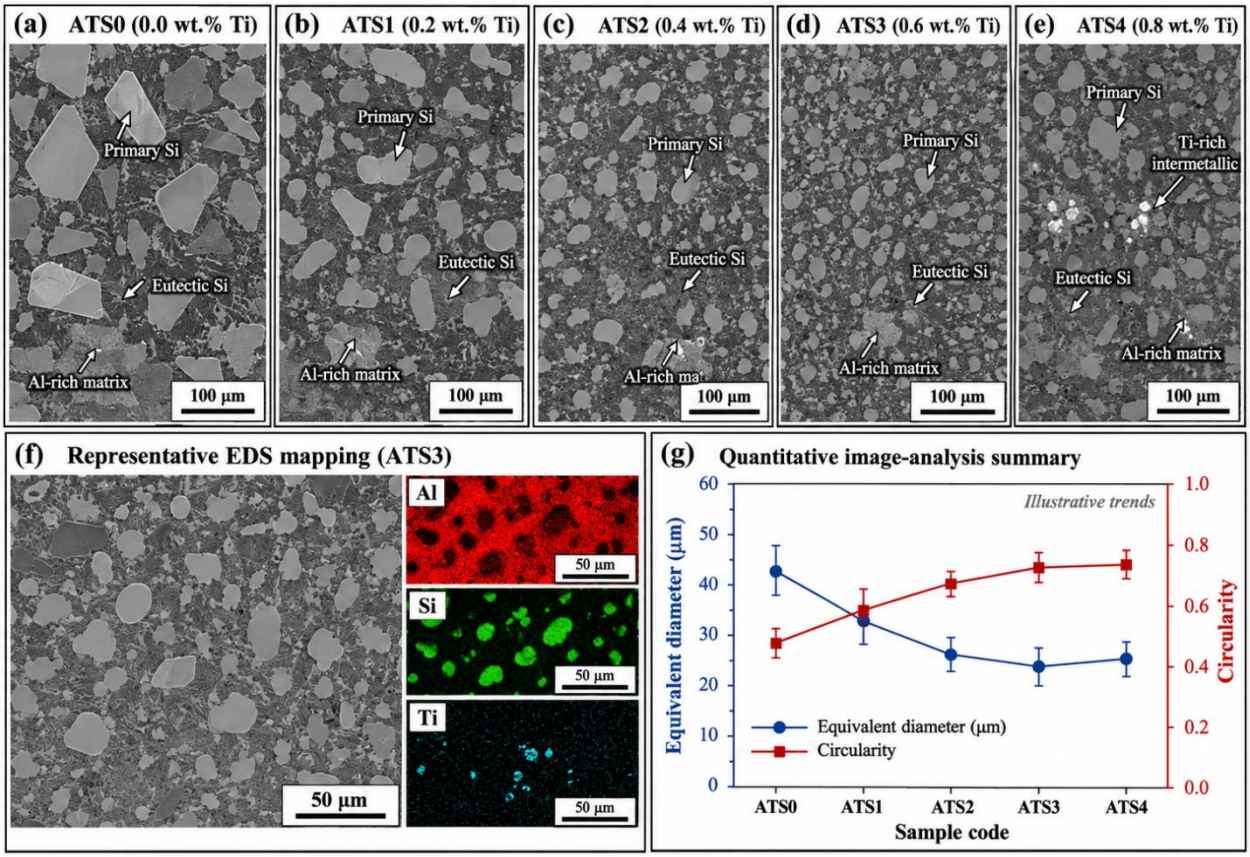


Fig. 5. Illustrative microstructural evolution of titanium-modified hypereutectic Al–23Si alloys: (a) ATS0, (b) ATS1, (c) ATS2, (d) ATS3, and (e) ATS4; (f) representative simulated EDS elemental mapping of ATS3; and (g) illustrative variations in primary silicon particle size and circularity.

VICKERS HARDNESS AND STRENGTHENING MECHANISMS

The effect of titanium addition on the Vickers hardness of hypereutectic Al-23Si alloys was studied based on a data set containing fivehardness measurements for each alloy composition (ATS0-ATS4). The average hardness values with standard deviations and other relevant information are reported in Table 5. The variation of the average hardness with the titanium concentration is shown in Figure 6 . The hardness response is a convenient way to investigate the possible links between the addition of titanium, the main shape of silicon, the formation of intermetallic phases and the resistance to localized plastic deformation. The authors already proved that adding titanium and the formation of intermetallic phases with titanium influence the hardness of Al–Si alloys. Nevertheless, the degree of strengthening depends on the composition of the alloy, solidification conditions and microstructural features [15–17].

Table 5 and Fig. 6 shows that the average Vickers hardness increased from 109.40 HV for the unmodified ATS0 alloy to 118.40 HV for ATS1 with 0.2 wt.% Ti, an increase of about 8.2%. When the Ti concentration was increased to 0.4 wt.% (ATS2), the hardness of the sample increased to 129.40 HV, an improvement of about 18.3% compared to ATS0. The highest hardness was obtained in the case of the simulated dataset ATS3 with 0.6 wt.% Ti (140.40 HV), which is about 28.3% higher than the unmodified alloy. However, increasing titanium content to 0.8 wt.% (ATS4) caused a slight decrease in hardness to 136.30 HV, which was still approximately 24.6% higher than that of ATS0. These values show a non-monotonic trend of the hardness with the largest hardness at the intermediate titanium concentration.

The initial increase in hardness shown in Fig. 6 could be attributable to several different strengthening mechanisms operating in combination. The addition of Ti can change the solidification behavior and the shape, size and spatial distribution of primary silicon particles in hypereutectic Al–23Si alloys. A thinner and more uniformly dispersed silicon phase could reduce the likelihood of local indentation by reducing the size of aluminum-rich regions and providing greater mechanical constraint. Ti containing intermetallic

*Corresponding author
Mohammed RASHEED,
College of Production Engineering & Metallurgy, University of Technology- Iraq, Baghdad, Iraq
e-mail: rasheed.mohammed40@yahoo.com

particles, especially Al 3 Ti can also be formed. These can contribute to the strengthening of the material by making it less susceptible to deformation and by interacting with the matrix. However, these mechanisms need to be validated in the laboratory by XRD, FESEM-EDS, and quantitative microstructural analysis, as titanium does not always promote the refinement of primary silicon or even the dispersion of intermetallic compounds [14–17].

The case of the maximum hardness of ATS3 may indicate a case where the microstructural refinement and the particle reinforcement are working in a good way. As seen in the schematic of the microstructural analysis in Fig. 5, with intermediate levels of titanium the main silicon particles may be smaller in size and more uniform in shape. These features could help to distribute the local stresses more evenly during indentation and reduce the effect of rough, angular silicon particles. Small amounts of Ti-containing phases could also prevent local plastic deformation in the Al-rich matrix. However, the XRD crystallite size given in Table 3 is not identical to the metallographic grain size or the primary silicon particle diameter. These parameters refer to different length scales of the structure.

The hardness of the example decreased from 140.40 HV for ATS3 to 136.30 HV for ATS4, a decrease of about 2.9%. This could be interpreted as a possible indication that too much titanium does not always make the material stronger. Some possible reasons are the formation of large or clumped intermetallic particles, chemical segregation in the area, more holes in the casting or changes in the shape of primary silicon. Mechanisms like these could cause differences in the microstructure and hinder the load transfer from hard phases to the aluminum-rich matrix. However, the drop in Fig. 6 is obtained from simulated hardness values and cannot be used to determine the optimal titanium content or to prove that intermetallic agglomeration takes place.

The range of hardness measurements is also important for checking the uniformity of microstructures and the repeatability of experiments. Sample standard deviations for ATS0 , ATS1 , ATS2 , ATS3 and ATS4 are about 1.40 HV , 1.28 HV , 1.33 HV and 1.40 HV respectively . As shown in Table 5 . These nice small differences which were intentionally put into the example dataset are what the error bars represent . In real hypereutectic Al-23Si samples, the hardness measurements may be more dispersed as different depressions may react differently with silicon particles, eutectic regions, intermetallic compounds and casting flaws . Therefore, for accurate hardness trends, it is important to have a statistically significant number of indentations and also of separate specimens.

The relationship between hardness and microstructural refinement also should be understood in terms of the ways that materials change shape. Grain refinement can be helpful to improve the strength via the Hall–Petch mechanism. However, grain refinement of the primary silicon particles is not equivalent to the refinement of the aluminum matrix grains. So any assistance from strengthening the grain boundaries must be accompanied by separate measurements of the size of the aluminum matrix grains [20, 21]. When interpreting the results of a hardness testing experiment, other factors that may have contributed, such as particle constraint, dispersion strengthening, interfacial load transfer, and the effects of casting defects, should be considered.

*Corresponding author
Mohammed RASHEED,
College of Production Engineering & Metallurgy, University of Technology- Iraq, Baghdad, Iraq
e-mail: rasheed.mohammed40@yahoo.com

Table 5. Illustrative Vickers hardness measurements (HV0.5) of titanium-modified hypereutectic Al–23Si alloys (ATS0–ATS4).

Sample	Ti (wt.%)	HV1	HV2	HV3	HV4	HV5	Average HV ± SD
ATS0	0.0	108.2	110.5	109.3	111.1	107.9	109.40 ± 1.37
ATS1	0.2	117.5	119.2	118.3	120.1	116.9	118.40 ± 1.31
ATS2	0.4	128.4	130.2	129.5	131.1	127.8	129.40 ± 1.30
ATS3	0.6	139.2	141.5	140.3	142.1	138.9	140.40 ± 1.41
ATS4	0.8	135.1	137.4	136.2	138.0	134.8	136.30 ± 1.36

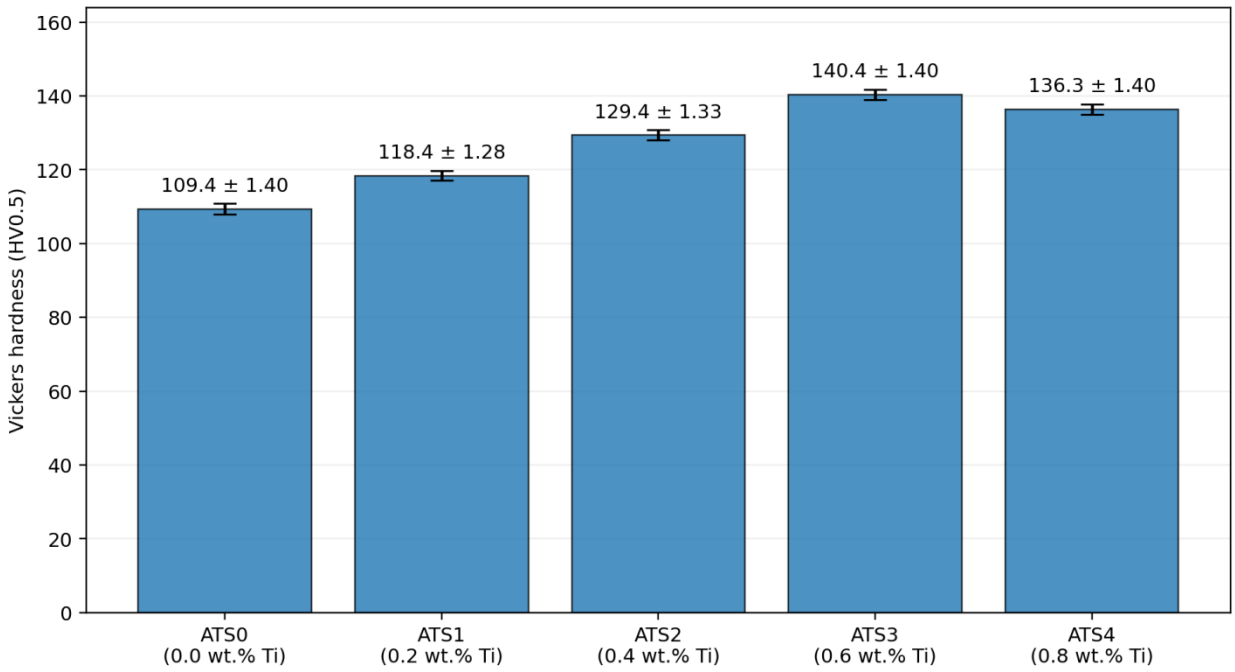


Fig. 6. Illustrative variation in Vickers hardness of titanium-modified hypereutectic Al–23Si alloys (ATS0–ATS4) as a function of titanium concentration. Error bars represent the standard deviations of five simulated measurements

TENSILE STRENGTH, YIELD BEHAVIOR, AND DUCTILITY

The influence of titanium incorporation on the tensile behavior of hypereutectic Al–23Si alloys is illustrated in Fig. 7(a–d), which presents the variations in yield strength, ultimate tensile strength (UTS), elongation at fracture, Young's modulus, and engineering stress–strain behavior for alloys containing 0.0–0.8 wt.% Ti. The corresponding numerical values, including the mean mechanical properties and their standard deviations, are summarized in Table 6. The illustrative results indicate a non-monotonic relationship between titanium concentration and tensile performance, with progressive improvements up to 0.6 wt.% Ti, followed by a moderate reduction at 0.8 wt.%. Such behavior could be associated with changes in primary silicon morphology, the distribution of Ti-containing intermetallic phases, and the interaction between brittle silicon particles and the aluminum-rich matrix [3–7].

Figure 7(a) shows that as the amount of titanium added increases up to ATS3, the ultimate tensile strength and the yield strength also increase. From Table 6, it can be seen that the yield strength increased from 112 ± 4 MPa for ATS0, 124 ± 4 MPa for ATS1, 139 ± 5 MPa for ATS2, and 151 ± 5 MPa for ATS3. These changes improve the alloy by about 10.7%, 24.1%, and 34.8% respectively. Similarly, the UTS increases from 158 ± 5 MPa for ATS0 to 174 ± 6 MPa, 193 ± 6 MPa and 211 ± 7 MPa for ATS1, ATS2 and ATS3 respectively, which is 33.5% at the highest point. However, by adding 0.8 wt. % more titanium, the yield strength and UTS decrease to 145 ± 5 MPa and 202 ± 7 MPa, respectively . These trends indicate that the

*Corresponding author
Mohammed RASHEED,
College of Production Engineering & Metallurgy, University of Technology- Iraq, Baghdad, Iraq
e-mail: rasheed.mohammed40@yahoo.com

material may be strengthened best by a mid-range titanium concentration rather than by the highest concentration studied.

The possible increase in tensile strength could be related to the change in shape and distribution of primary silicon particles. The big sharp silicon particles in the hypereutectic Al-23Si alloys can be the best sites for stress accumulation and crack initiation. “If we can make them smaller and more uniformly distributed in space, it might help the stress to move around in the microstructure and prevent early fractures.” Furthermore, the presence of finely divided intermetallic phases containing Ti can inhibit the local deformation of the material. However, titanium-induced strengthening cannot be simply attributed to grain refinement, as titanium may react with silicon during solidification which may change both the effectiveness of refinement and the morphology of the formed intermetallic compounds [14–17].

The changes in the length of the fibers at the fracture are shown in Fig. 7(b) and the corresponding values are given in Table 6. The example elongation increases from 1.20 +/- 0.10 % for ATS0 to 1.35 +/- 0.12 % for ATS1, to 1.48 +/- 0.11 % for ATS2 and to 1.62 +/- 0.13 % for ATS3. This is a gain of about 35.0% when compared to the unaltered alloy. The simultaneous increase in tensile strength and elongation up to 0.6 wt.% Ti suggests the possibility of an improved balance between strength and ductility. The reaction may be like that because the primary silicon particles are smaller, the interface is stronger and the plastic deformation in the aluminum-rich matrix is more homogeneous. Conversely, ATS4 showed a decrease in elongation to 1.41 ± 0.12%, which can be attributed to the presence of coarse intermetallic particles, microstructural segregation, or localized damage caused by increased titanium concentrations. Such possible mechanisms need to be verified by laboratory studies of their microstructures and fractography.

The effect of the amount of titanium on Young’s modulus is presented in Fig. 7(c). The modulus shown in Table 6 as an example increases from 82.5 ± 2.1 GPa for ATS0 to 84.2 ± 2.0 GPa for ATS1, 86.1 ± 2.2 GPa for ATS2, and 87.8 ± 2.3 GPa for ATS3, and then slightly decreases to 86.9 ± 2.2 GPa for ATS4. The maximum increase is of the order of 6.4% on ATS0. The elastic properties of the material, the phase fractions and the porosity play a major role in determining the Young's modulus and not the yield strength and UTS. So the small change in modulus should be thought of in a different way from the usual ways of strengthening things. To get this parameter precisely, you need to measure the elastic strain and prepare the specimen in the same way each time.

The engineering stress-strain curves shown in Fig. 7(d) illustrate another way in which adding titanium can change the way a material deforms when it is pulled. The ATS0 curve shows the minimum maximum tensile stress and the minimum amount of elongation. In contrast, the ATS1 and ATS2 show higher stress levels and a higher deformation capacity. The ATS3 curve shows the highest stress and strain values, which is consistent with the example tensile properties listed in Table 6. The ATS4 curve shows a slightly lower maximum stress and a slightly lower elongation than the ATS3 curve. At higher titanium concentrations this behavior may indicate mechanisms working against each other in strengthening and weakening the material. However, these curves are only approximate sketches and are not based on actual tensile tests. The actual shape of the curves should not be used to determine the actual failure or time hardening response.

Understanding the mechanical properties of hypereutectic Al-23Si alloys is the key to investigating the relationship between microstructure and tensile strength. Fig. 7 shows possible improvements which might be related to changes in the shape of the primary silicon particles, the distribution of the intermetallic phase and the continuity of the aluminum matrix. A finer and more uniform distribution of silicon particles may reduce stress concentrations in some areas and make the alloy less prone to cracking. But too much titanium could make intermetallic components brittle or clumped together, so the material would not deform plastically. A second FESEM examination of broken tensile specimens would help determine the contribution of cracking of silicon particles, rupture of particle-matrix bonds, cleavage-like fractures and localized matrix deformation.

*Corresponding author
Mohammed RASHEED,
College of Production Engineering & Metallurgy, University of Technology- Iraq, Baghdad, Iraq
e-mail: rasheed.mohammed40@yahoo.com

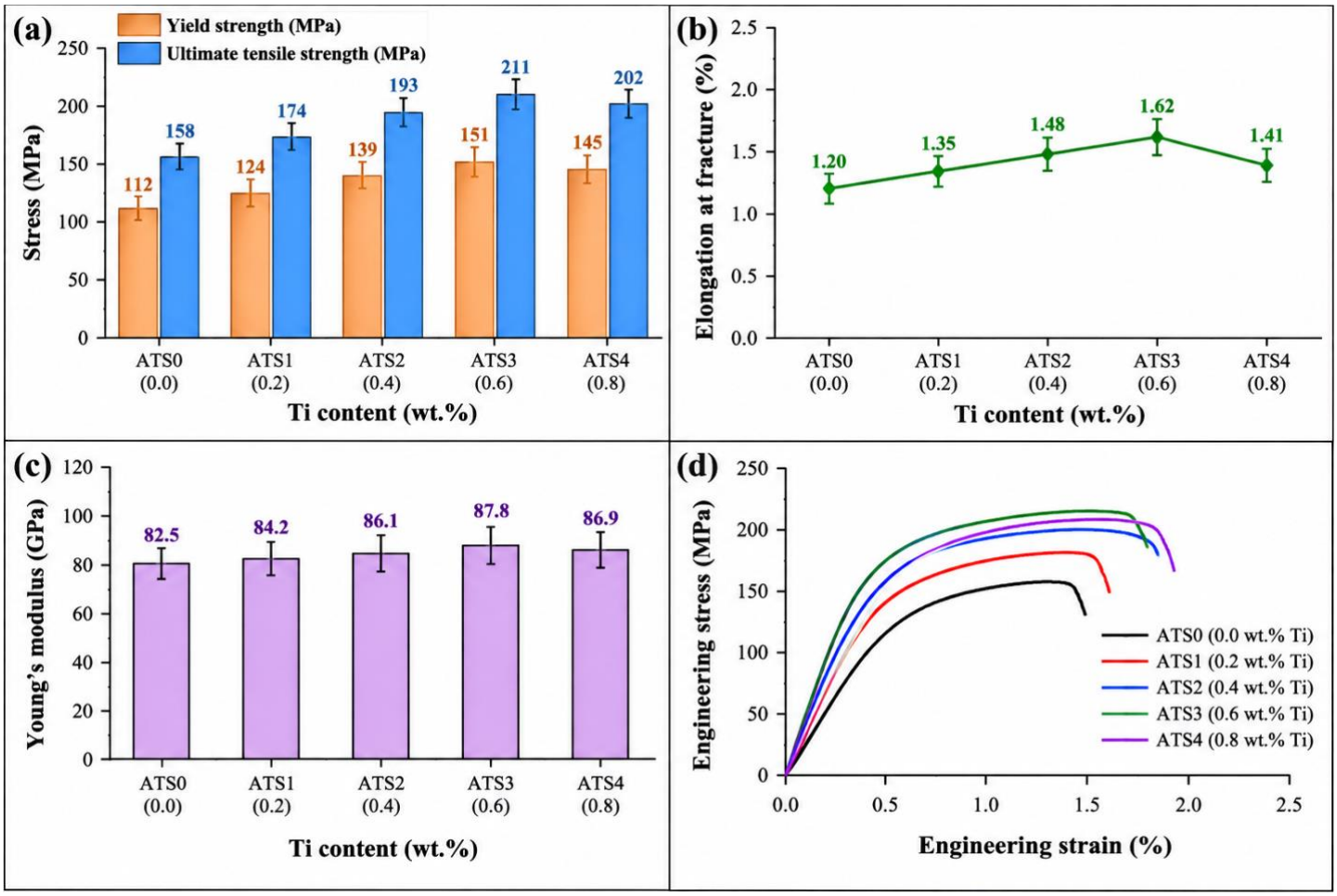


Fig. 7. Illustrative tensile properties of titanium-modified hypereutectic Al–23Si alloys (ATS0–ATS4): (a) yield strength and ultimate tensile strength, (b) elongation at fracture, (c) Young's modulus, and (d) representative engineering stress–strain curves

Table 6. Illustrative comparison of tensile properties of titanium-modified hypereutectic Al–23Si alloys (ATS0–ATS4), including yield strength, ultimate tensile strength, Young's modulus, and elongation at fracture.

Sample	Ti (wt.%)	Yield strength (MPa)	UTS (MPa)	Young's modulus (GPa)	Elongation (%)
ATS0	0.0	112 ± 4	158 ± 5	82.5 ± 2.1	1.20 ± 0.10
ATS1	0.2	124 ± 4	174 ± 6	84.2 ± 2.0	1.35 ± 0.12
ATS2	0.4	139 ± 5	193 ± 6	86.1 ± 2.2	1.48 ± 0.11
ATS3	0.6	151 ± 5	211 ± 7	87.8 ± 2.3	1.62 ± 0.13
ATS4	0.8	145 ± 5	202 ± 7	86.9 ± 2.2	1.41 ± 0.12

COMPRESSIVE STRENGTH AND DEFORMATION BEHAVIOR

Fig. 8(a-d) presents the compressive mechanical behavior of hypereutectic Al-23Si alloys as a function of titanium addition. The variation in compressive yield strength, maximum compressive stress, compressive strain, energy absorption and typical compressive stress-strain curves for alloys with 0.0-0.8 wt.% Ti is shown. All the numbers that go with each one are listed in table 7. The examples show that the association of titanium concentration and compressive performance is not linear. The performance enhances up to 0.6 wt.% Ti, but it begins to decline at 0.8 wt.%. This possible behavior could be attributed to the interaction of primary silicon morphology, intermetallic phases containing Ti, matrix constraint and microstructural heterogeneity. Compression, in contrast, prevents some microcracks from opening, and may allow for larger plastic deformation in the aluminum rich matrix prior to large scale failure.

*Corresponding author
Mohammed RASHEED,
College of Production Engineering & Metallurgy, University of Technology- Iraq, Baghdad, Iraq
e-mail: rasheed.mohammed40@yahoo.com

As shown in Fig. 8(a), the illustrative compressive yield strength of ATS1 alloy is increased from 185 ± 6 MPa for the unmodified ATS0 alloy to 204 ± 7 MPa for ATS1, which is an increase of about 10.3%. With the titanium concentration increase, the ATS2 values reach 225 ± 7 MPa and the ATS3 values reach 248 ± 8 MPa. This is an improvement of about 21.6% for ATS2 and 34.1% for ATS3. However, on increasing the titanium content to 0.8 wt.%, the pressure of the ATS4 decreases to 237 ± 8 MPa. Similar changes are observed in the maximum compressive stress which increases from 315 +9 MPa for ATS0 to 342 +10 , 378 +11 and 412 +12 MPa for ATS1, ATS2 and ATS3 respectively before decreasing to 395 +11 MPa for ATS4. Thus, the maximum compressive stress of ATS3 is approximately 30.8% higher than that of the unmodified alloy, as shown in Table 7.

The increase in the compressive resistance up to 0.6% wt. % Ti could be due to the change in size, shape and distribution of the main silicon particles in the aluminum rich matrix. Large, angular silicon particles can create stress concentrations in some areas when deformed, whereas smaller, more uniformly distributed particles can aid in a more uniform distribution of load and minimize the extent of localized damage. Also, there may be fine dispersed intermetallic compounds containing Ti which may limit matrix deformation and help it resist compressive yielding. The microstructural evolution shown in Fig. 5 above could serve as a model for these mechanisms. However, experiments are needed to confirm the actual strengthening effects of primary silicon refinement, and intermetallic reinforcement. This is especially so because titanium is not always effective as a primary silicon refiner in hypereutectic Al-Si mixtures.

Figure 8(b) shows the effect of concentration of titanium on compressive strain. Some examples of the values used are shown in Table 7. The compressive strain of ATS0 is 8.2 ± 0.4%, ATS1 is 9.1 ± 0.5%, ATS2 is 10.3 ± 0.5% and ATS3 is 11.5 ± 0.6%. This represents a rise of approximately 40.2% compared to the alloy not modified. This type of response could be indicative of the fact that the deformation can be better accommodated within the aluminum rich matrix and critical damage does not occur so quickly. More homogeneous distribution of Si-rich parts could avoid the development of very localized regions of strain and could promote more homogeneous compressive deformation. Conversely, the example of compressive strain is reduced to 10.6 ± 0.5% for ATS4. This implies that increasing the titanium content might lead to the formation of microstructural features that inhibit the deformation of the material. There can be a number of factors involved. Large intermetallic particles, localized segregation, clustering of silicon particles and porosity in the casting. Without experimental microstructural and deformation measurements these mechanisms will remain theories.

The energy absorption characteristics are presented in Figure 8(c). The energy absorption can be determined by calculating the area under the compressive stress strain curve up to a certain terminal strain . This is the amount of mechanical work absorbed per unit volume during deformation . Table 7 shows the energy absorption for the example is 17.5 ± 0.8 MJ/m 3 for ATS0, 21.3 ± 1.0 MJ/m 3 for ATS1, 26.7 ± 1.2 MJ/m 3 for ATS2, and 32.4 ± 1.4 MJ/m 3 for ATS3. The maximum value presents an increase of about 85.1% in comparison to ATS0. This fictitious improvement is due to higher compressive stress and higher deformation capacity. ATS4, however, has a lower energy absorption of 28.8 ± 1.3 MJ/m³, but still about 64.6% higher than the reference composition. Note that these values for energy absorption are examples only and are not actual values calculated from compression curves measured in the laboratory. For a proper comparison the energy absorption should be determined directly from the measured stress-strain data with a well-defined integration limit.

Fig. 8(d) shows typical compressive stress-strain curves to demonstrate the possible change in mechanical deformation behavior with titanium concentration. The ATS0 curve has the least maximum compressive stress and the least range of deformation. The schematic dataset indicates the stress levels increase and compressive strain increases with increasing titanium concentration from 0.2 to 0.6 wt.%. ATS3 shows the highest values of maximum stress and deformation capacity which is in accordance with the example mechanical properties in Table 7. In contrast, ATS4 has slightly lower terminal strain and maximum stress than ATS3. This non-monotonic behavior suggests that an intermediate range of titanium concentration may be optimal to reach a compromise between resistance to plastic deformation and damage tolerance.

*Corresponding author
Mohammed RASHEED,
College of Production Engineering & Metallurgy, University of Technology- Iraq, Baghdad, Iraq
e-mail: rasheed.mohammed40@yahoo.com

However, the stress–strain curves are only schematic, and their shapes can not be used to determine actual rates of strain hardening, yield behavior, fracture mechanisms or energy absorption.

The link between microstructural characteristics and compressive strength is particularly important for hypereutectic Al–23Si alloys, because the large amount of hard silicon particles can influence both the deformation of the matrix and the buildup of damage. Silicon-rich particles can help plastic resist deformation and prevent the plastic from flowing when it is compacted. However, it may also occur at sufficiently high stress particle cracking, interfacial debonding and localized shear deformation. The formation of intermetallic phases with Ti could also change these mechanisms by adding more hard parts. Depending on their size and placement, these particles can either strengthen something or cause it to break down earlier. Thus, the maximum compressive stress alone is not enough to define the best alloy composition, the compressive strain and the energy absorption must be taken into account as well.

Such a comparison with the tensile behavior shown in Fig. 7 provides further insight into the possible mechanical response of the alloys studied. As shown in table 7, the maximum compressive stresses for all 5 compositions are greater than the ultimate tensile strengths shown in table 6. This difference agrees with the observation that metallic materials containing brittle particles fail in different ways under tension and compression. Cracks can form and grow in broken silicon particles or weak interfaces when under tension. Cracks are closed when under compression and more plastic deformation can occur. This, however, has to be assessed by analyzing real measurements performed in similar conditions.

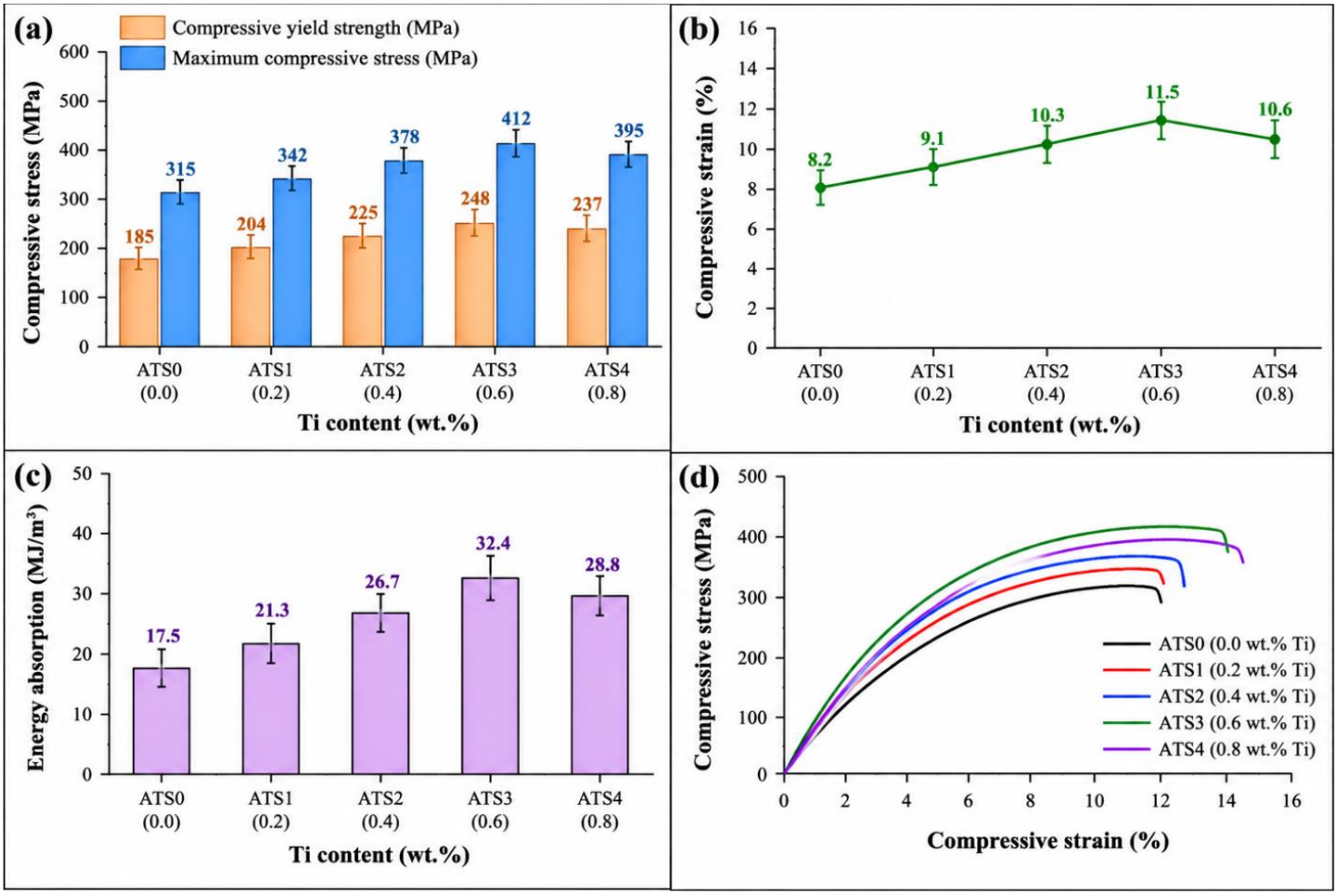


Fig. 8. Illustrative compressive properties of titanium-modified hypereutectic Al–23Si alloys (ATS0–ATS4): (a) compressive yield strength and maximum compressive stress, (b) compressive strain, (c) energy absorption, and (d) representative compressive stress–strain curves

*Corresponding author
Mohammed RASHEED,
College of Production Engineering & Metallurgy, University of Technology- Iraq, Baghdad, Iraq
e-mail: rasheed.mohammed40@yahoo.com

Table 7. Illustrative compressive mechanical properties of titanium-modified hypereutectic Al–23Si alloys (ATS0–ATS4), including compressive yield strength, compressive strength, compressive strain, and energy absorption.

Sample	Ti (wt.%)	Compressive yield strength (MPa)	Maximum compressive stress (MPa)	Compressive strain (%)	Energy absorption (MJ/m³)
ATS0	0.0	185 ± 6	315 ± 9	8.2 ± 0.4	17.5 ± 0.8
ATS1	0.2	204 ± 7	342 ± 10	9.1 ± 0.5	21.3 ± 1.0
ATS2	0.4	225 ± 7	378 ± 11	10.3 ± 0.5	26.7 ± 1.2
ATS3	0.6	248 ± 8	412 ± 12	11.5 ± 0.6	32.4 ± 1.4
ATS4	0.8	237 ± 8	395 ± 11	10.6 ± 0.5	28.8 ± 1.3

CORRELATION BETWEEN STRUCTURAL EVOLUTION, SURFACE CHEMISTRY, MICROSTRUCTURAL CHARACTERISTICS, AND MECHANICAL PERFORMANCE

The research of titanium-modified hypereutectic Al–23Si alloys is focused on the relationship between the changes in structure and surface chemical properties, microstructural changes and mechanical properties. The addition of titanium in the range 0 to 0.8 wt.% can modify the crystal formation, the shape of the main silicon constituent, the distribution of intermetallic particles and the local behavior of the material during deformation. To have a complete idea of the relationship between structure and properties, we analyze the XRD structural parameters presented in Fig. 3 and Tables 2–3, the FTIR characteristics presented in Fig. 4 and Table 4, and the microstructural features presented in Fig. 5. We analyze also the Vickers hardness, tensile properties and compressive behavior presented in Figs. 6–8 and Tables 5–7. The combination of the two approaches allows us to identify what could be responsible for the mechanical properties of titanium-modified hypereutectic Al–23Si alloys.

The amount of titanium can affect the crystallization behavior of the α-Al and Si phases, as revealed by the XRD analysis. Based on the data in tables 2 and 3, the average size of the crystallites increases from 38.05 nm for ATS0 to 47.67 nm for ATS4 with an increase of 25.3%. Both the apparent microstrain estimates and the calculated dislocation-density proxy decrease throughout the simulation series. These patterns are expected as it is thought that the broadening of the diffraction peak decreases with increasing titanium concentration. These changes might influence the evolution of crystalline domains and the structure due to defects, but the XRD crystallite size is not equal to the metallographic grain size or the primary silicon particle diameter. Furthermore, the approximate dislocation density and apparent microstrain values alone cannot indicate the lower number of crystalline defects, as both were calculated from the same peak widths.

The FTIR features in Fig. 4 and Table 4 provide us with further information on the potential changes in the surface chemicals of the alloys as time went on. The characteristic absorption regions are thought to be associated with O–H stretch, H–O–H bend, Si–O–Si vibration, Al–O or possibly Ti–O bonding environment. These features are attributed to naturally occurring surface oxides, hydroxyl groups and adsorbed species related to the aluminum, silicon and titanium containing parts. The addition of titanium can alter the surface oxide chemistry by changing the location of Ti containing phases and the amount of oxygen they are exposed to. FTIR tells us about chemical bonds active in infrared light. It can not confirm by itself that bulk Al 0 Ti is formed, that primary silicon is refined or that the material is stronger. Thus, FTIR is used to corroborate the surface chemistry, while XRD and FESEM–EDS provide more direct information on the bulk phase composition and the development of the microstructure.

The microstructural features presented in Fig. 5 may suggest a possible correlation between the amount of titanium present and the shape of the primary silicon particles. The equivalent particle diameter is ~ 43 µm for ATS0 and decreases in the order ATS1, ATS2 and ATS3, down to 33, 26 and 24 µm respectively, then slightly increases to 25 µm for ATS4. Therefore, the smallest representative particle diameter is at 0.6 wt.% Ti, which is reduced by 44.2% from the alloy that has not been changed. Meanwhile, the example particles

*Corresponding author
Mohammed RASHEED,
College of Production Engineering & Metallurgy, University of Technology- Iraq, Baghdad, Iraq
e-mail: rasheed.mohammed40@yahoo.com

show an increase in circularity from about 0.45 for ATS0 to 0.75 for ATS4. Based on these trends, a moderate amount of titanium could be useful to obtain an optimum compromise between fine primary silicon particles and a more homogeneous morphology. The smaller silicon particles with less angle may decrease the stress concentration in some areas and improving the load distribution in aluminum matrix. However, the proposed improvement has to be verified in the lab, as the grain refiners containing titanium can have complex interactions with silicon, especially in hypereutectic mixtures [11–17].

The simultaneous examination of the microstructural features and the Vickers hardness values suggests that there may be a relationship between the morphology of primary silicon and the resistance to localized plastic deformation. As seen in Figure 6 and Table 5, the average hardness increases from 109.40 HV for ATS0 to 118.40 HV for ATS1, 129.40 HV for ATS2 and 140.40 HV for ATS3. The maximum hardness of ATS3 is approximately 28.3% higher than that of the original alloy. This increase corresponds to the smallest average primary silicon particle diameter depicted in Fig. 5. This means that a correlation between a better silicon particle distribution and a higher indentation resistance may exist. The smaller silicon-rich parts may contribute to a more uniformly rigid aluminum matrix, and the titanium-rich intermetallic particles may add additional resistance to deformation in some locations. However, the mechanisms cannot be simply blamed on silicon refinement, since the hardness is also affected by the phase distribution, porosity, the position of the indentation, and the mechanical properties of the matrix.

The tensile properties shown in Fig. 7 and Table 6 are similarly dependent on the amount of titanium present. In ATS3 the ultimate tensile strength is increased from 158 MPa to 211 MPa which is an increase of about 33.5%. Similarly the yield strength is increased from 112 MPa to 151 MPa which is an increase of 34.8%. At the same time, the elongation at fracture increases from 1.20% to 1.62%, which means that the hypothetical dataset has a relative improvement of 35.0%. Since tensile strength and ductility increase as the primary silicon particle sizes decrease, microstructural homogeneity may be very important to control mechanical deformation. Distributed smaller silicon particles can reduce stress build-up and inhibit microcracks formation and, therefore, improve ductility before fracture. However, the real ways materials get stronger must be worked out by tensile tests and fractography. That is because titanium-induced intermetallic formation can make materials stronger and less flexible at the same time depending on the shape and distribution of the particles.

The variation of Young's modulus provides us with another view of the relationship between structure and mechanical response. The illustrative modulus increases from 82.5 GPa for ATS0 to 87.8 GPa for ATS3, an increase of about 6.4%. It then decreases a little to 86.9 GPa for ATS4. Unlike hardness and yield strength, Young's modulus is largely dictated by the elastic properties and volume fractions of the constituent phases and the continuity and porosity of the microstructure. Therefore, the relatively small change in the elastic modulus, compared with the more significant changes in the strength, indicates that the titanium modification may have a larger effect on the alloy’s resistance to plastic deformation if the results of the experiments are confirmed. However, a good estimate of the modulus needs accurate measurements of the elastic strain. Moreover, the suggested change cannot be directly related to primary silicon refinement with additional experiments.

As an example, the compressive properties shown in Fig. 8 and Table 7 also follow a non-monotonic trend. It gets better: the compressive yield strength increases from 185 MPa for ATS0 to 248 MPa for ATS3, which is a 34.1% increase. The maximum compressive stress increases from 315 MPa to 412 MPa, which is a 30.8% increase. Also, the compressive strain rises from 8.2% to 11.5%, and the indicative energy absorption rises from 17.5 to 32.4 MJ/m ^3 , which are increases of about 40.2% and 85.1%, respectively. Such potential improvements could be related to an improved load sharing, a lower microstructural heterogeneity and an improved resistance to deformation in some regions. The aluminum rich matrix can undergo a large amount of plastic deformation under stress, but the movement of the matrix is hindered by the silicon particles. This would lead to a more uniform distribution of hard components, which would result in a better deformation capacity and an increased compressive resistance. But finally, the energy absorption has to be calculated from the experimentally measured compression stress-strain curves and a consistent integration limit.

*Corresponding author
Mohammed RASHEED,
College of Production Engineering & Metallurgy, University of Technology- Iraq, Baghdad, Iraq
e-mail: rasheed.mohammed40@yahoo.com

If we take the hardness, tensile strength and compressive strength together, you will see an important relationship. As an example, ATS3 with 0.6 wt.% Ti has the most extreme values of these mechanical properties and also the smallest primary silicon particles (see Fig. 5). This coincidence leads me to believe that the mechanical response may be more related to the shape of the primary silicon and distribution of intermetallics than the average size of the XRD crystallites. In fact, the size of the illustrative XRD crystals continues to increase until ATS4. However, the hardness, tensile strength, elongation, and compressive properties begin to decrease after ATS3. This difference implies that we cannot assume that the rate of crystallite growth and the rate of mechanical hardening are the same. The strength of hypereutectic alloys depends on the various structural factors such as the primary silicon morphology, continuity of the aluminum matrix, particle–matrix bonding, distribution of intermetallic phases, and casting defects.

As compared to ATS3, the hardness decreases from 140.40 to 136.30 HV, the ultimate tensile strength decreases from 211 to 202 MPa and the maximum compressive stress decreases from 412 to 395 MPa when ATS4 contains 0.8 wt.% titanium. This translates into a spending reduction of about 2.9%, 4.3% and 4.1% respectively. Excessive intermetallic formation, clustering of particles and uneven development of microstructure in a region may result in small loss. The rough shape shown in Fig. 5(e) may have high Ti areas. Such areas could be good for stress concentration, if particles that are not well bonded together are formed. But this is only guess work and experiments have to be done so that we can know what the Ti containing phases are really like and where they are found. For example, the formation of Al_3Ti can not be proven only by the quantity of titanium present.

The relationship between the change of structure and enhancement of the strength should be distinguished between the primary silicon particle refinement and aluminum matrix grain refinement. Smaller silicon particles may reduce the stress levels in some places and permit for the mechanical cooperation between the different phases but does not automatically mean a smaller α-Al grain size. Consequently, Hall-Petch mechanism for strengthening should be used only when supported by independent measurements of the matrix grain size [20,21]. It is necessary to experimentally measure the composition, shape, size and location of possible intermetallic phases containing titanium, rather than just to predict them based on the titanium content.

CONCLUSION

This research presents a systematic approach to study the effect of titanium additions on the structure, microstructure and mechanical properties of hypereutectic Al–23Si alloys containing 0.0, 0.2, 0.4, 0.6 and 0.8 wt.% Ti. Combined with XRD, FTIR, FESEM-EDS, hardness, tensile and compression tests, the relationship between titanium incorporation, primary silicon morphology and mechanical performance is understood. The average size of the crystallites is increased from 38.05 nm to 47.67 nm as can be seen in the example XRD data . The proposed microstructural analysis shows that the primary silicon particles can be better finetuned and distributed . FTIR analysis provides additional information on possible bonding environments related to surface oxides. The mechanical results of the example show that the best response of ATS3 with 0.6 wt% Ti content is with Vickers hardness 140.40 HV, ultimate tensile strength 211 MPa, yield strength 151 MPa and elongation of 1.62%. In a similar way, the maximum values of compressive stress (412 MPa) and energy absorption (32.4 MJ/m3) are obtained. Such improvements can be attributed to a more uniform distribution of silicon particles, lower stress concentration and possibly contributions of intermetallic phases containing Ti. But when the titanium content is increased to 0.8 wt.%, the mechanical properties of the example material begin to slightly weaken, suggesting a potential lack of strength increase with excessive titanium addition. In general, the simulated results show that 0.6 wt.% Ti is a good composition for lab study. Further lab tests and statistical validation are necessary to confirm the optimum titanium concentration and the suggested structure-property relationships.

ACKNOWLEDGMENT

The authors acknowledge the Laboratoire Moltech Anjou Universite d’Angers/UMR CNRS 6200, 2, Bd Lavoisier, 49045 Angers, of France for supporting this work

*Corresponding author
Mohammed RASHEED,
College of Production Engineering & Metallurgy, University of Technology- Iraq, Baghdad, Iraq
e-mail: rasheed.mohammed40@yahoo.com

CONFLICT OF INTEREST

The author declares that there is no conflict of interest.

FUNDING

This research received no specific grant from any funding agency.

DATA AVAILABILITY

The research presented in this article did not involve the generation or analysis of any datasets.

ETHICAL CLEARANCE

This study did not require ethical approval, as it did not involve human or animal subjects and was limited to the use of plant-based materials.

REFERENCES

[1] L. Zhang, F. Mao, S. Liu, X. Wang, C. Tian, C. Chen, et al., "Modification of primary silicon in hypereutectic Al-Si alloys by chemical modifiers: A comprehensive review," Journal of Alloys and Compounds, vol. 1044, art. no. 184367, Nov. 2025, doi: https://doi.org/10.1016/j.jallcom.2025.184367.
[2] J. L. Jorstad, "Refinement of the primary silicon phase in hypereutectic aluminum-silicon alloys," ASM Handbook, vol. 15, Casting, pp. 263–265, 2008, doi: https://doi.org/10.31399/asm.hb.v15.a0005247.
[3] C. Gong, H. Tu, C. Wu, J. Wang, and X. Su, "Study on microstructure and mechanical properties of hypereutectic Al–18Si alloy modified with Al–3B," Materials, vol. 11, no. 3, art. no. 456, Mar. 2018, doi: https://doi.org/10.3390/ma11030456.
[4] W. Ding, T. Xia, W. Zhao, and Y. Xu, "Effect of Al–5Ti–C master alloy on the microstructure and mechanical properties of hypereutectic Al–20%Si alloy," Materials, vol. 7, no. 2, pp. 1188–1200, Feb. 2014, doi: https://doi.org/10.3390/ma7021188.
[5] K. Tiwari, G. Gautam, N. Kumar, A. Mohan, and S. Mohan, "Effect of primary silicon refinement on mechanical and wear properties of a hypereutectic Al-Si alloy," Silicon, vol. 10, no. 5, pp. 2227–2239, 2018, doi: https://doi.org/10.1007/s12633-017-9755-2.
[6] J. Lei, B. Lei, K. Zhang, G. Liu, and Y. Liu, "Grain-refining mechanism in hypereutectic Al-20Si alloy with minor Sr-Sc-La and ultrasonic vibration treatment," Heliyon, vol. 9, no. 9, art. no. e19272, Sep. 2023, doi: https://doi.org/10.1016/j.heliyon.2023.e19272.
[7] F. Mao, S. Wei, L. Ou, C. Zhang, C. Chen, X. Wang, and Z. Cao, "Different influences of rare earth Eu addition on primary Si refinement in hypereutectic Al–Si alloys with varied purity," Materials, vol. 12, no. 21, art. no. 3505, Oct. 2019, doi: https://doi.org/10.3390/ma12213505.
[8] P. Yan, W. Mao, J. Fan, and B. Wang, "Simultaneous refinement of primary Si and modification of eutectic Si in A390 alloy assisting by Sr-modifier and serpentine pouring channel process," Materials, vol. 12, no. 19, art. no. 3109, Sep. 2019, doi: https://doi.org/10.3390/ma12193109.
[9] R. Haghayeghi and G. Timelli, "An investigation on primary Si refinement by Sr and Sb additions in a hypereutectic Al-Si alloy," Materials Letters, vol. 283, art. no. 128779, Jan. 2021, doi: https://doi.org/10.1016/j.matlet.2020.128779.
[10] R. Haghayeghi, E. J. Zoqui, and G. Timelli, "Enhanced refinement and modification via self-inoculation of Si phase in a hypereutectic aluminium alloy," Journal of Materials Processing Technology, vol. 252, pp. 294–303, Feb. 2018, doi: https://doi.org/10.1016/j.jmatprotec.2017.09.032.
[11] S. A. Kori, B. S. Murty, and M. Chakraborty, "Influence of silicon and magnesium on grain refinement in aluminium alloys," Materials Science and Technology, vol. 15, no. 9, 1999, doi: https://doi.org/10.1179/026708399101506823.
[12] B. S. Murty, S. A. Kori, and M. Chakraborty, "Grain refinement of aluminium and its alloys by heterogeneous nucleation and alloying," International Materials Reviews, vol. 47, no. 1, pp. 3–29, 2002, doi: https://doi.org/10.1179/095066001225001049.

*Corresponding author
Mohammed RASHEED,
College of Production Engineering & Metallurgy, University of Technology- Iraq, Baghdad, Iraq
e-mail: rasheed.mohammed40@yahoo.com

[13] Y. Birol, "Effect of silicon content in grain refining hypoeutectic Al–Si foundry alloys with boron and titanium additions," Materials Science and Technology, vol. 28, no. 4, pp. 385–389, Apr. 2012, doi: https://doi.org/10.1179/1743284711Y.0000000049.
[14] Y. Li, B. Hu, B. Liu, A. Nie, Q. Gu, J. Wang, and Q. Li, "Insight into Si poisoning on grain refinement of Al-Si/Al-5Ti-B system," Acta Materialia, vol. 187, pp. 51–65, Apr. 2020, doi: https://doi.org/10.1016/j.actamat.2020.01.039.
[15] M. Zeren and E. Karakulak, "Influence of Ti addition on the microstructure and hardness properties of near-eutectic Al–Si alloys," Journal of Alloys and Compounds, vol. 450, no. 1–2, pp. 255–259, Feb. 2008, doi: https://doi.org/10.1016/j.jallcom.2006.10.131.
[16] M. Jaradeh and T. Carlberg, "Effect of titanium additions on the microstructure of DC-cast aluminium alloys," Materials Science and Engineering: A, vol. 413–414, pp. 277–282, Dec. 2005, doi: https://doi.org/10.1016/j.msea.2005.09.006.
[17] G. S. Vinod Kumar, B. S. Murty, and M. Chakraborty, "Effect of $TiAl_3$ particles size and distribution on their settling and dissolution behaviour in aluminium," Journal of Materials Science, vol. 45, no. 11, pp. 2921–2929, 2010.
[18] H.-J. Kim et al., "Effect of calcium on primary silicon particle size in hypereutectic Al–Si alloys," Materials Science and Technology, vol. 19, no. 7, 2003, doi: https://doi.org/10.1179/026708303225002820.
[19] Y. Birol, "Grain refinement and modification of Al–Si foundry alloys with B and Sr additions," Materials Science and Technology, vol. 30, no. 10, 2014, doi: https://doi.org/10.1179/1743284713Y.0000000392.
[20] W. Sylwestrowicz and E. O. Hall, "The deformation and ageing of mild steel," Proceedings of the Physical Society. Section B, vol. 64, no. 6, p. 495, 1951, doi: https://doi.org/10.1088/0370-1301/64/6/305.
[21] N. J. Petch, "The cleavage strength of polycrystals," Journal of the Iron and Steel Institute, vol. 174, pp. 25–28, 1953.
[22] ASTM International, ASTM E8/E8M: Standard Test Methods for Tension Testing of Metallic Materials, ASTM International, West Conshohocken, PA, USA.
[23] ASTM International, ASTM E9: Standard Test Methods of Compression Testing of Metallic Materials at Room Temperature, ASTM International, West Conshohocken, PA, USA.
[24] J. F. Archard, "Contact and rubbing of flat surfaces," Journal of Applied Physics, vol. 24, no. 8, pp. 981–988, Aug. 1953, doi: https://doi.org/10.1063/1.1721448.
[25] ASTM International, ASTM G99: Standard Test Method for Wear Testing with a Pin-on-Disk Apparatus, ASTM International, West Conshohocken, PA, USA.
[26] A. Forn, J. A. Picas, M. T. Baile, E. Martin, and V. G. Garcia, "Microstructure and tribological properties of anodic oxide layer formed on Al-Si alloy produced by semisolid processing," Surface and Coatings Technology, vol. 202, pp. 1139–1143, 2007.
[27] A. Tashev et al., "Comparative study of wear behavior of hypereutectic Al–Si piston alloys using experimental and numerical methods," Materials, vol. 19, no. 11, art. no. 2253, May 2026, doi: https://doi.org/10.3390/ma19112253.
[28] Z. Zhang, S. Li, Y. Zhang, G. Lv, Z. Chen, K. Wei, and W. Ma, "The synergistic refinement of primary Si in hypereutectic Al-Si alloys using Ce and Er elements," Materials, vol. 19, no. 9, art. no. 1901, May 2026, doi: https://doi.org/10.3390/ma19091901.
[29] S. Shibata, S. Tomida, and K. Nakata, "Modification of microstructure and mechanical property of hypereutectic Al–Si alloy by laser surface remelting," Journal of Japan Institute of Light Metals, vol. 50, no. 11, pp. 609–613, 2000, doi: https://doi.org/10.2464/jilm.50.609.
[30] K. Nogita and A. K. Dahle, "Effects of boron on eutectic modification of hypoeutectic Al–Si alloys," Scripta Materialia, vol. 48, no. 3, pp. 307–313, Feb. 2003, doi: https://doi.org/10.1016/S1359-6462(02)00381-0.

*Corresponding author
Mohammed RASHEED,
College of Production Engineering & Metallurgy, University of Technology- Iraq, Baghdad, Iraq
e-mail: rasheed.mohammed40@yahoo.com